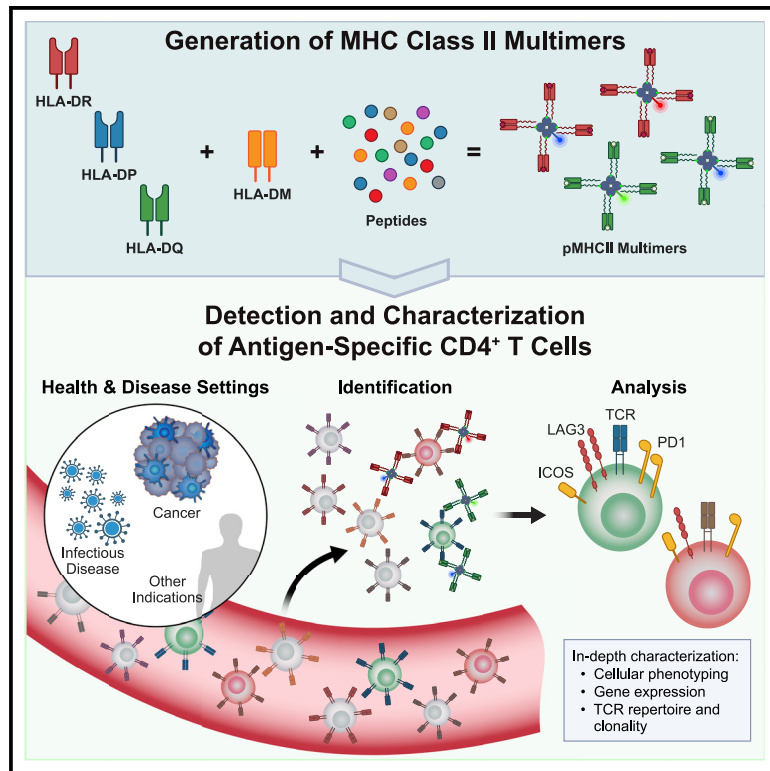


A universal MHCII technology platform to characterize antigen-specific CD4⁺ T cells

Graphical abstract



Authors

Rohit Vyasamneni, Victoria Kohler, Binisha Karki, ..., Richard B. Gaynor, Meghan E. Bushway, John R. Srouji

Correspondence

meghan.bushway@biontech.us (M.E.B.), john.srouji@biontech.us (J.R.S.)

In brief

Identifying and characterizing all potential CD4⁺ T cell specificities is difficult in many personalized and disease contexts. Vyasamneni and Kohler et al. develop a robust platform of MHCII protein production, custom epitope peptide loading, and multimer-based identification, and validate its application in infectious disease and cancer immunotherapy settings.

Highlights

- A method for generating functional MHC class II protein alleles
- Universal MHC class II epitope loading catalyzed by soluble HLA-DM
- Multimerization of pMHCII antigen allows for CD4⁺ T cell identification
- Broad characterization of antigen-specific CD4⁺ T cells in diverse disease settings



Article

A universal MHCII technology platform to characterize antigen-specific CD4⁺ T cells

Rohit Vyasamneni,^{1,2} Victoria Kohler,^{1,2} Binisha Karki,¹ Gauri Mahimkar,¹ Ekaterina Esaulova,¹ Jonathan McGee,¹ Daniel Kallin,¹ Joong Hyuk Sheen,¹ Dewi Harjanto,¹ Miles Kirsch,¹ Asaf Poran,¹ Jesse Dong,¹ Lakshmi Srinivasan,¹ Richard B. Gaynor,¹ Meghan E. Bushway,^{1,*} and John R. Srouji^{1,3,*}

¹BioNTech US, Inc., 40 Erie Street, Cambridge, MA 02139, USA

²These authors contributed equally

³Lead contact

*Correspondence: meghan.bushway@biontech.us (M.E.B.), john.srouji@biontech.us (J.R.S.)

<https://doi.org/10.1016/j.crmeth.2022.100388>

MOTIVATION CD4⁺ T cells are critical for productive immune responses. Identifying and characterizing antigen-specific CD4⁺ T cells are therefore crucial to assessing disease progression and developing potent therapeutic interventions. However, there is enormous diversity in T cell receptors (TCRs) and MHCII antigen sequences and specificities, both within an individual and across the human population, making it difficult to identify their antigen specificity at high throughput and sufficient depth to gain biological insight. Currently available methods either do not support analyses across multiple alleles/epitopes or obscure the cellular phenotype of the cells. To address this technological deficiency, we developed a robust platform of MHCII protein production, custom epitope peptide loading, and multimer-based identification and validated its application in infectious disease and cancer immunotherapy settings. This biochemical and immunological toolbox could be used to identify any antigen-specific CD4⁺ T cell population in any disease indication.

SUMMARY

CD4⁺ T cells are critical to the immune system and perform multiple functions; therefore, their identification and characterization are crucial to better understanding the immune system in both health and disease states. However, current methods rarely preserve their *ex vivo* phenotype, thus limiting our understanding of their *in vivo* functions. Here we introduce a flexible, rapid, and robust platform for *ex vivo* CD4⁺ T cell identification. By combining MHCII allele purification, allele-independent peptide loading, and multiplexed flow cytometry technologies, we can enable high-throughput personalized CD4⁺ T cell identification, immunophenotyping, and sorting. Using this platform in combination with single-cell sorting and multimodal analyses, we identified and characterized antigen-specific CD4⁺ T cells relevant to COVID-19 and cancer neoantigen immunotherapy. Overall, our platform can be used to detect and characterize CD4⁺ T cells across multiple diseases, with potential to guide CD4⁺ T cell epitope design for any disease-specific immunization strategy.

INTRODUCTION

CD4⁺ T cells are an important component of the adaptive immune system, exerting multiple direct and indirect functions to drive immune responses.^{1,2} CD4⁺ T cells are activated upon encounter with their cognate antigen displayed on the surface of professional antigen-presenting cells (APCs) by major histocompatibility complex class II (MHCII) molecules.³ Upon activation, CD4⁺ T cells can help B cells generate durable and high-affinity antibodies, activate cytotoxic CD8⁺ T cells, suppress immune activation through T regulatory subsets,

and directly kill tumor and virally infected cells.^{1,4} These functions are critical to driving robust immune responses in many settings,^{1,4} such as viral infection and vaccination,⁴ and more recently in the context of the ongoing COVID-19 pandemic.⁵ In the field of cancer immunotherapy, there has been a recent focus on targeting MHCII epitopes to help orchestrate CD4⁺ T cell-driven tumor rejection, which has been demonstrated in both nonclinical and clinical settings.^{6–9} Therefore, it is imperative to identify antigen-specific CD4⁺ T cells to guide downstream functional characterization.



Current methods for identifying antigen-specific CD4⁺ T cells predominantly rely on antigen recall/stimulation and/or require enrichment prior to characterization, all of which can distort the *ex vivo* phenotype of these cells.^{10,11} Furthermore, these methods rely on the upregulation of surface activation induced markers (AIM),¹⁰ which can lead to a biased understanding of the CD4⁺ T cell compartment because only cells that effectively upregulate the markers of interest, including non-specific bystander cells, are captured and analyzed. Not only do current methods obscure the phenotype of antigen-specific T cells, but they also lack sufficient sensitivity to detect multiple distinct antigen-specific populations in a single sample. The most direct means of *ex vivo* identification and analysis of multiple antigen-specific CD4⁺ T cell populations has been MHCII multimer analysis.

Reliable methods for MHCII allele production and epitope loading have proven elusive, due to the structural and biological nuances of MHCII, thus hindering the widespread and personalized application of multimer technologies. Two polypeptide chains, at least one of which is highly polymorphic, heterodimerize to form the MHCII peptide-binding groove, leading to a large combinatorial diversity of alleles in the human population. In addition, unlike the length limitations for MHCI epitopes, MHCII epitopes are presented with their termini protruding out of an open-ended peptide-binding pocket, resulting in long epitopes with potentially multiple binding registers¹² that hinder accurate binding predictions. In contrast to MHCI multimer and supporting technologies, there is not a single robust means of MHCII allele protein production and epitope loading. To produce soluble alleles, most investigators either directly refold MHCII ectodomain polypeptide chains (derived from *Escherichia coli* inclusion bodies) with free epitope^{13,14} or express folded MHCII with a covalently linked epitope peptide in insect or mammalian cells.^{15–17} These approaches, however, suffer from low throughput and/or lack validation across many alleles and epitopes and no current technologies offer an on-demand and allele-independent epitope loading strategy. To empower the personalized *ex vivo* analysis and characterization of antigen-specific CD4⁺ T cells, robust and on-demand MHCII allele production, allele restriction deconvolution, epitope loading and affinity quantification, and detection methods are needed.

Here we present a robust platform for rapid and high-throughput CD4⁺ T cell multimer analysis. Using this technology, we identified antigen-specific CD4⁺ T cells in the context of COVID-19 and multiple cancer indications. In the context of COVID-19, we were able to detect CD4⁺ T cells specific to multiple epitopes derived from the spike, membrane, and nucleocapsid proteins, demonstrating that multiple viral genes generate central and effector memory CD4⁺ T cells with an antigen-experienced phenotype. When coupled to high-dimensional immunophenotyping and applied to cancer patients treated with a personalized vaccine, our MHCII platform demonstrated that vaccine-induced neoantigen-specific CD4⁺ T cells were clonal, durable, and predominantly of a Th1 memory phenotype, suggesting these cells may have an anti-tumor function.¹ In conclusion, we present a robust platform for the *ex vivo* investigation of antigen-specific CD4⁺ T cells across multiple disease indications.

RESULTS

A robust platform for transient expression and purification of loadable MHCII alleles

MHCII alleles rapidly adopt a non-receptive conformation for peptide loading in the absence of a loaded peptide.^{18,19} Therefore, to produce soluble MHCII alleles capable of downstream epitope loading, we leveraged the documented success of covalently linking a cleavable placeholder peptide to the beta allele during production.^{15,17} In alignment with the general understanding of MHCII biogenesis and cellular trafficking (previously reviewed^{20,21}), the class II-associated invariant chain peptide (CLIP) and variants thereof served as a placeholder peptide for almost all alleles (Table S1). To aid in rapid and high-throughput allele production, we designed all DNA expression vectors for transient transfection and protein secretion from Expi293F suspension culture (Figures 1A and 1B). For almost all alleles produced, gel filtration chromatography revealed high- and low-molecular-weight post-translationally modified (PTM) populations; in all cases, only the low PTM population was used for multimer staining (Figure 1C). Using this production platform, we purified 48 MHCII alleles to an average yield of ~40 mg/L transfected culture, corresponding to >80% European allele coverage^{22–24} (Figure 1D and Table S1).

Soluble HLA-DM catalyzes rapid and complete peptide exchange across HLA-DP, DQ, DR, and murine alleles

On-demand and universal MHCII epitope loading is a key challenge to the widespread application of CD4⁺ multimer technologies in diverse disease contexts. To overcome this, we sought to replicate the natural ability of HLA-DM to load MHCII alleles with epitopes. In APCs, full-length HLA-DM associates with full-length MHCII to unload the CLIP and promote the loading of high-affinity epitopes.^{20,21} Because almost all soluble MHCII alleles purified above are loaded with CLIP, we hypothesized that recombinant soluble HLA-DM (HLA-sDM, see STAR Methods and Figures S1A–S1C) could promote on-demand epitope loading under similar *in vivo* (i.e., acidic) conditions.

To demonstrate epitope loading and measure the effect of various catalysts over time, we developed a fluorescence polarization (FP) assay to displace cleaved placeholder peptide with allele-specific high-affinity FITC-labeled probes (Figure 2A and Table S2). Except for some HLA-DP alleles, acidic reaction buffer alone did not promote FITC-probe loading for most alleles (Figures 2B and S2), with HLA-DQ and murine alleles being particularly recalcitrant. Small-molecule chaperones for MHCII loading have been previously described^{25,26}; we tested if the commonly used n-octyl-beta-D-glucopyranoside (OG) could function as a universal catalyst.^{17,27,28} OG only promoted FITC-probe loading on a subset of HLA-DR and -DP alleles (Figures 2B and S2). In contrast, HLA-sDM successfully promoted FITC-probe loading across all tested alleles at a reasonable rate (<24 h) to support on-demand loading and routine analysis (Figures 2B and S2).

We further modified the FP assay to quantify the relative affinity of epitopes. By mixing high-affinity FITC-probes with specific epitopes in the presence of HLA-sDM, we could measure the relative affinity (half maximal inhibitory concentration [IC₅₀]) and

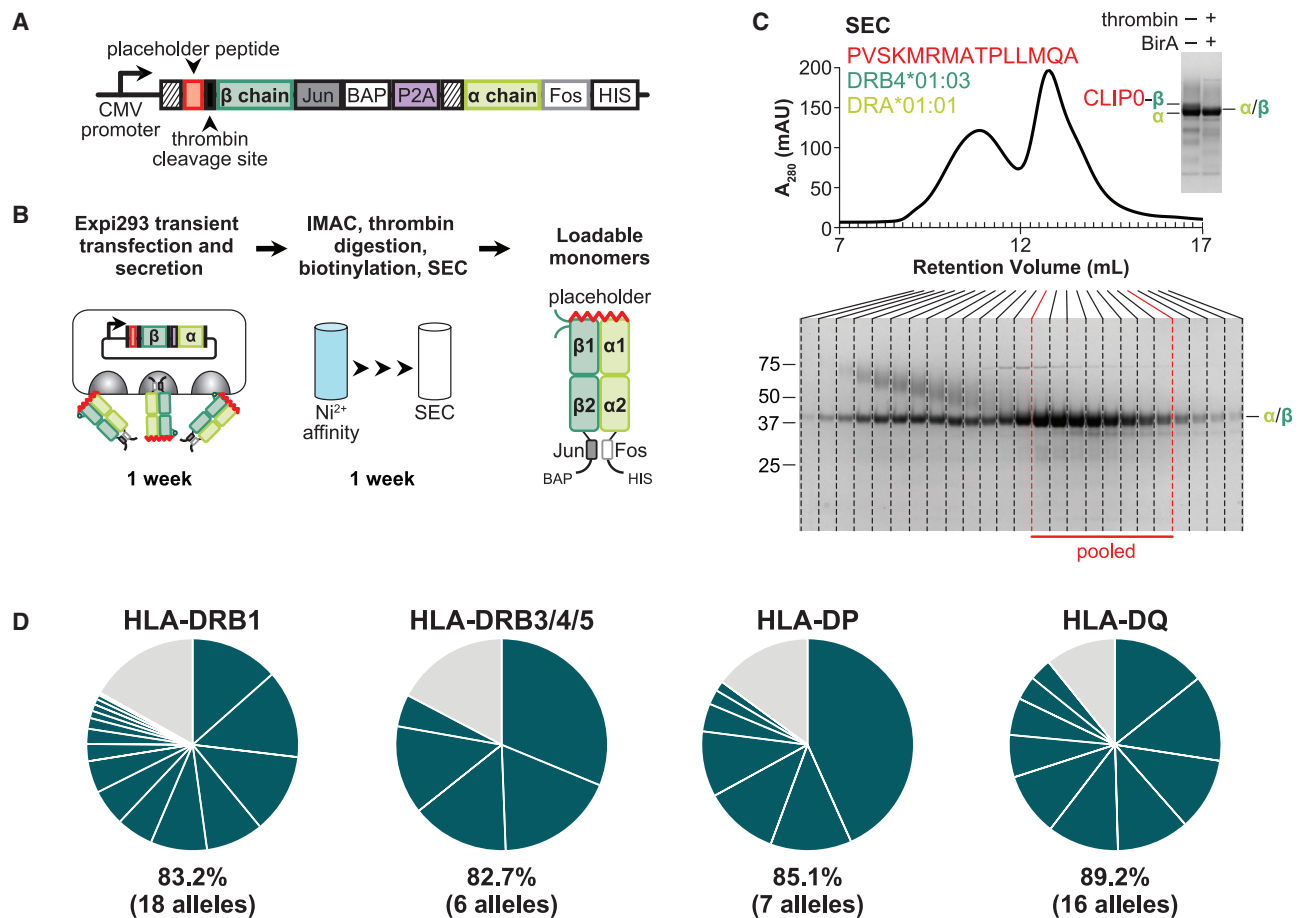


Figure 1. MHCII alleles covering a broad swath of the human population are produced as soluble heterodimers with cleavable peptide placeholders from transiently transfected human cells

(A) Soluble MHC class II DNA construct design (see STAR Methods and Table S1 for details).

(B) Protein expression and purification strategies (with timelines) to generate MHCII protein ready for epitope loading, multimerization, and flow cytometry staining.

(C) Example protein purification of biotinylated (via BirA) and thrombin-digested HLA-DRB4*01:03/DRB1*01:01 heterodimer bound to the CLIP0 placeholder (PVSKMRMATPLLMQA). Gel filtration chromatogram and SDS-PAGE gel shown, with purification fractions subsequently pooled for epitope loading and flow cytometry staining indicated in red.

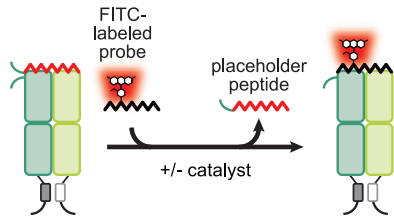
(D) European allele frequencies^{22–24} of MHCII alleles for which protein purification has been demonstrated (see Table S1).

allele restriction for any given epitope (Figure 2C). We applied this methodology to a set of predicted epitopes derived from SARS-CoV-2 spike (S) antigen^{29,30} and successfully quantified the relative binding affinity of S epitopes against HLA-DRB1*07:01, DPB1*04:01/DPA1*01:03, and DQB1*06:02/DQA1*01:02 (Figure 2D and Table S2). Overall, we have successfully deployed this FP-competition assay for all alleles tested thus far (29 out of 48) across HLA-DP, DQ, DR, and murine H2 (Table S3).

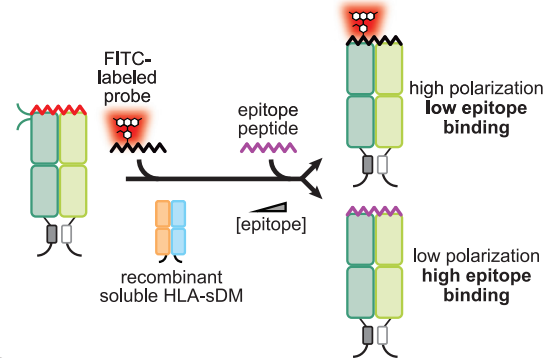
Finally, we sought to understand the degree of peptide loading mediated by HLA-sDM. We performed an experiment in which we isolated FITC-probe loaded MHCII protein after HLA-sDM catalyzed exchange via anti-FITC immunoprecipitation (IP) followed by SDS-PAGE analysis of the IP samples (Figures 2E and 2F). Placeholder-loaded MHC II alleles underwent HLA-sDM loading in the presence or absence of a FITC-labeled

peptide, were purified by size exclusion chromatography, and immunoprecipitated with an anti-FITC monoclonal antibody. For all three DP, DQ, and DR alleles tested, HLA-sDM was able to drive complete FITC-peptide loading such that no unloaded MHCII allele was detectable in the IP flowthrough (Figure 2F). To assess the stability and function of purified MHCII protein after long-term frozen storage at -80°C , we tested the epitope loading capability and aggregation propensity of one DP allele. We compared a freshly purified sample and a >1-year frozen aliquot of the same allele (DPB1*02:01/DPA1*01:03) and found both to have the same affinity for a FITC-probe (Figure S3A) and when analyzed via analytical SEC did not show any aggregation, which would be expected at 5.5 min (Figure S3B). In addition, we analyzed the binding affinity and aggregation profile for three additional DP, DQ, and DR alleles and found no significant effect on binding performance

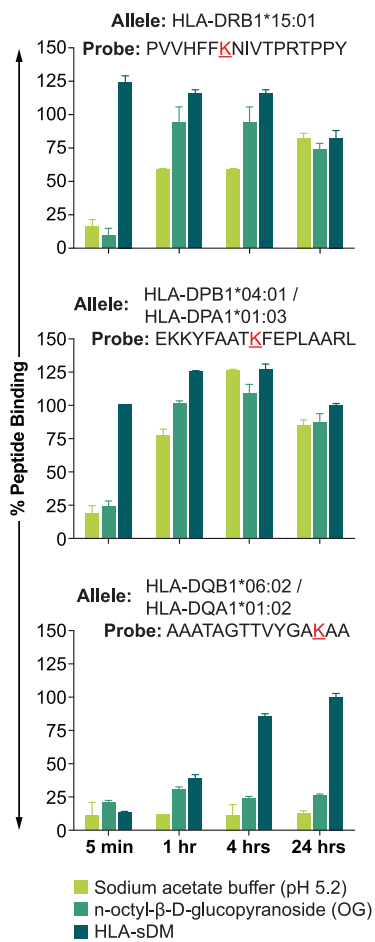
A Probe Binding Assay



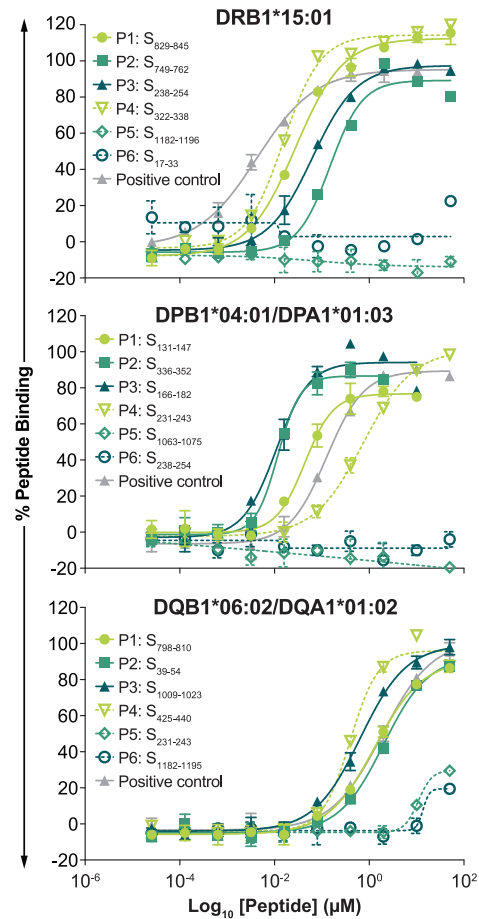
C Epitope Competition Assay



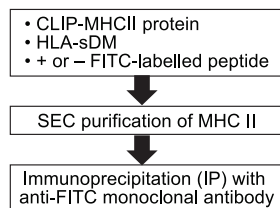
B



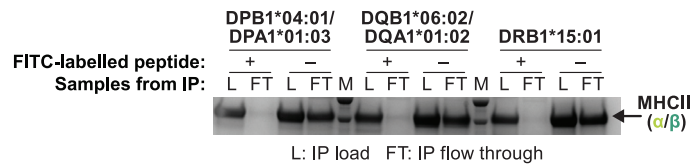
D



E



F



(legend on next page)

or aggregation after repeated freeze and thaw cycles (Figures S3C and S3D). In summary, HLA-sDM catalyzes universal epitope loading on all tested MHCII alleles and the FP assay can be used to determine relative epitope binding affinity, thus supporting the application of this technology to identify antigen-specific CD4⁺ T cells.

pMHCII tetramers can detect multiple antigen specificities in a single sample with high sensitivity

Having demonstrated the ability to produce soluble MHCII alleles and load them with desired epitopes, we next sought to establish robust detection using flow cytometry. Because CD4⁺ T cell receptors (TCRs) are thought to have low affinity toward their peptide-MHCII (pMHCII) antigens,^{31,32} we wanted to determine if tetramerizing soluble pMHCII would be sufficient for antigen-specific CD4⁺ T cell staining. We stained healthy donor peripheral blood mononuclear cells (PBMCs) stimulated with the cytomegalovirus (CMV) pp65₁₁₆₋₁₂₉ epitope using either fluorescently labeled streptavidin (SA) or Klickmer (Immudex) multimer scaffolds, both conjugated to biotinylated and CMV-epitope loaded HLA-DRB1*01:01 “monomers.” Klickmers are composed of a fluorescently labeled dextran scaffold decorated with SA for conjugating pMHCII monomers (maximum potential valency of 28 pMHCII/scaffold), yielding a high-avidity staining reagent for detecting low-affinity CD4⁺ TCRs. When compared with Klickmers of different valencies (i.e., monomer concentrations), pMHCII SA-tetramers were able to detect the antigen-specific CD4⁺ T cell population at an equivalent frequency and slightly higher staining index (Figure S4A), indicating that our pMHCII tetramers are sufficient for staining antigen-specific CD4⁺ T cells.

Next, we sought to understand the limit of sensitivity for pMHCII tetramer staining. To generate a multi-epitope sample, we induced *ex vivo* responses in healthy donor PBMCs to MHCII epitopes from influenza (HA1₃₀₆₋₃₁₈), CMV (pp65₁₁₆₋₁₂₉), and HIV (Gag₂₆₂₋₂₇₆). Using unstimulated PBMCs from the same donor, we serially diluted the stimulated samples before staining to assess sensitivity (Figure S4B). Based on the diluted samples and low background staining with an irrelevant CLIP-MHCII tetramer, we determined that the limit of sensitivity is ≥ 10 events and a tetramer-positive frequency of $\geq 0.001\%$ (Figure S4B).

Because clinical samples are limited and contain many T cell reactivities, we evaluated the ability to simultaneously identify

more than one antigen-specific CD4⁺ T cell population from a single sample. To this end, we leveraged the demonstrated success of combinatorial coding.^{33,34} Using the same viral multi-epitope stimulated samples described above, we compared tetramer frequencies using multi-epitope combinatorial coding versus single-epitope approaches (see STAR Methods). Across all antigens, the tetramer frequencies remained consistent between both staining approaches, indicating that combinatorial coding of pMHCII tetramers does not hinder the detection of multiple antigen-specific CD4⁺ T cells (Figure S4C). As a final confirmation of staining specificity, we tested pMHCII tetramers using uninduced healthy donor PBMCs to ensure they specifically recognize CD4⁺ T cells. EBV-positive healthy donor PBMCs were stained with DRB1*07:01 tetramers loaded with EBNA2₂₈₀₋₂₉₀ peptide. Tetramer staining was only detected on CD4⁺ T cells and not among CD8⁺ T cells (Figure S4D).

pMHCII tetramers enable identification and characterization of SARS-CoV-2 antigen-specific CD4⁺ T cells from convalescent COVID-19 donors

Because CD4⁺ T cells play critical roles in the response to viral infections, we sought to identify and characterize SARS-CoV-2-specific CD4⁺ T cells from convalescent COVID-19 PBMCs using our MHCII tetramer platform (Table S4). We investigated spike (S)-, nucleocapsid (N)-, and membrane (M)-derived epitopes that either we predicted^{29,30} or were reported to be reactive^{35,36} in convalescent donors (see Table S5). Epitope/allele pairs were verified using the above-described FP assay prior to tetramer staining of convalescent COVID-19 PBMCs. SARS-CoV-2-specific CD4⁺ T cells were found in all five donors tested, including an immunodominant spike epitope (S₁₆₆₋₁₈₂)³⁷; in one donor (#51861), we simultaneously detected five unique specificities (Figures 3A, S5A and S5B). Overall, four out of five donors produced CD4⁺ T cells specific to at least two viral proteins, and two donors generated responses to all three proteins tested, suggesting that our loadable MHCII platform could detect the full range of CD4⁺ T cell antigen specificities generated upon natural SARS-CoV-2 infection.

To further characterize SARS-CoV-2 antigen-specific CD4⁺ T cells, we analyzed phenotypic and functional expression markers in three donors (#50833, #51861, and #53202) via flow cytometry. All antigen-specific CD4⁺ T cells, regardless of the specificity, were predominantly of central and effector memory phenotypes (Figures 3B and S5C). Furthermore, when compared

Figure 2. Soluble HLA-DM catalyzes rapid, on-demand, and universal MHCII peptide epitope loading

(A) Probe binding assay, whereby an MHCII allele bound to a cleaved placeholder peptide is emptied and reloaded with a high-affinity FITC-labeled peptide probe under catalyzed or uncatalyzed reaction conditions.

(B) Binding of FITC-probes was measured across three (un)catalyzed conditions via fluorescence polarization at four time points (see STAR Methods). Percent peptide binding was normalized to the 24-h HLA-sDM catalyzed condition (SD shown). Data are represented as mean \pm SD. FITC conjugation sites are underlined in red (see Table S2).

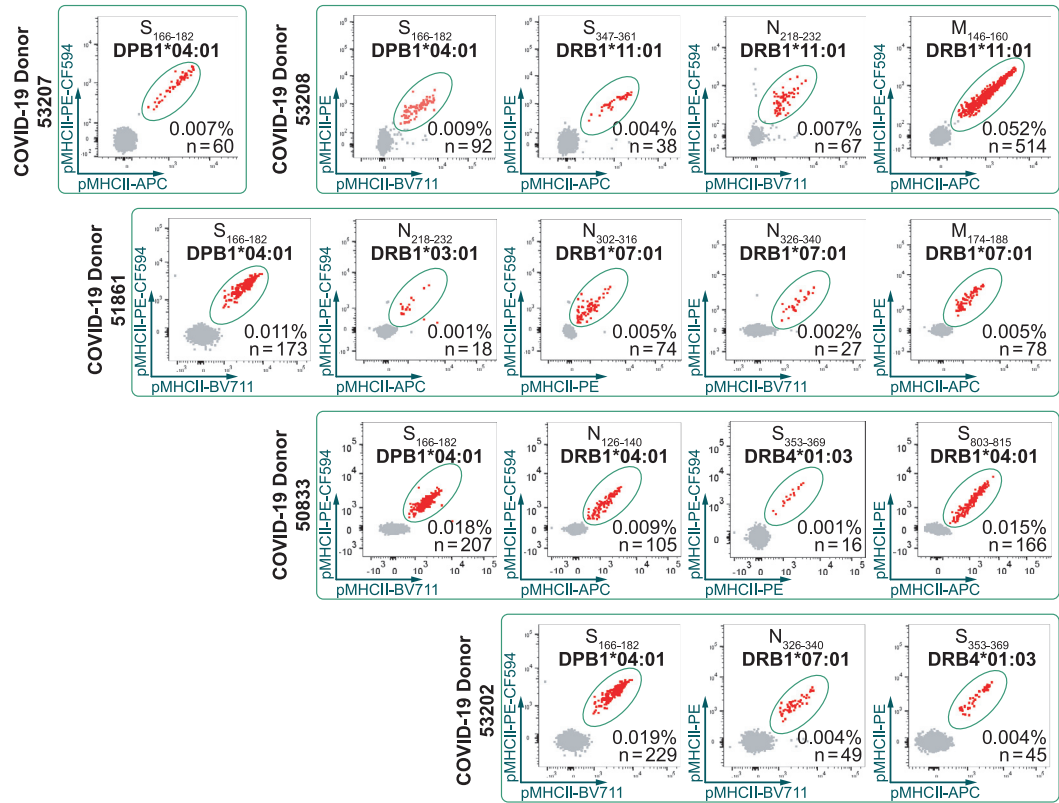
(C) Epitope competition assay, where fluorescent polarization is measured to quantify epitope peptide IC₅₀ (affinity), and allele restriction under HLA-sDM catalyzed conditions.

(D) Dose response IC₅₀ curves of predicted²⁹ SARS-CoV-2 spike (S)-derived epitopes. For each allele, predicted binders (P1-P4), non-binders (P5-P6), and a positive control were competed against an FITC-probe. Peptide binding was measured via fluorescence polarization after 24-h incubation (see STAR Methods and Table S3; SD shown). Data are represented as mean \pm SD.

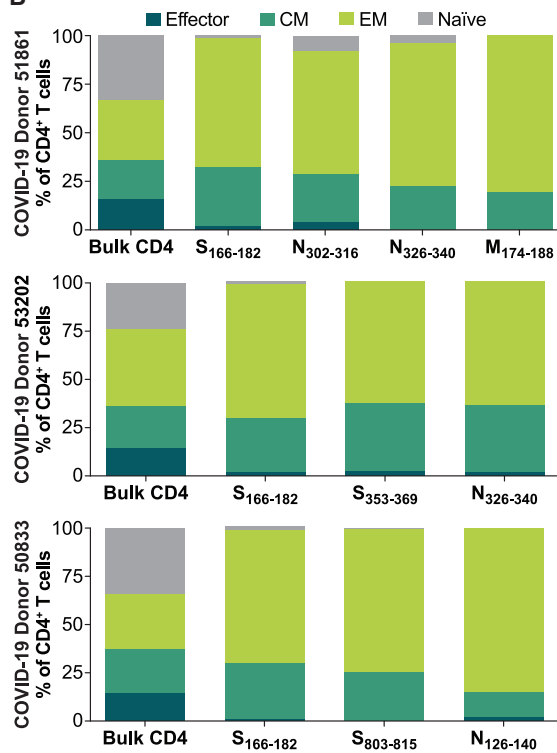
(E) Experimental schematic of peptide exchange and anti-FITC immunoprecipitation used to determine the extent of HLA-sDM-catalyzed peptide loading.

(F) SDS-PAGE analysis of the anti-FITC immunoprecipitation load (L) and flowthrough (FT) samples corresponding to three HLA alleles processed as shown in (E). SDS-PAGE gel has been cropped to just the region containing the unfolded MHCII chains; note that MHCII α and β chains co-migrate.

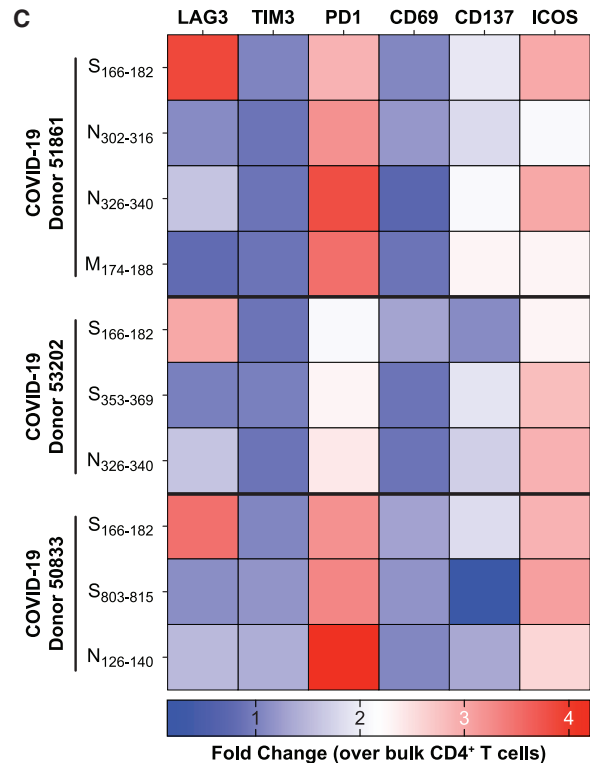
A



B



C



(legend on next page)

with bulk CD4⁺ T cells, antigen-specific cells upregulated ICOS and PD1 expression (Figure 3C). Interestingly, while TIM3 expression was not upregulated on antigen-specific populations, CD4⁺ T cells that recognized the immunodominant S₁₆₆₋₁₈₂ epitope showed a marked upregulation in LAG3 expression (Figure 3C), suggesting that CD4⁺ T cells specific to this region may be functionally distinct from other SARS-CoV-2-specific CD4⁺ T cells. The ability to identify and phenotypically characterize multiple SARS-CoV-2-specific CD4⁺ T cells may provide additional insights into their function in the context of natural infection or vaccination to COVID-19 and other infectious diseases.

pMHCII tetramers allow for detailed phenotypic and TCR profile analyses of neoantigen-specific CD4⁺ T cells from vaccinated metastatic cancer patients

Given the importance of CD4⁺ T cells in anti-tumor responses and clinical outcomes,^{6-9,38-43} we applied our MHCII technology to identify and phenotypically characterize *ex vivo* antigen-specific CD4⁺ T cells in metastatic cancer patients. We evaluated neoantigen-specific CD4⁺ T cells in peripheral blood from a group of metastatic cancer patients (one lung cancer [L7], one melanoma [M23], and two bladder cancer patients [B9, B10]) with measurable disease treated with a checkpoint inhibitor (anti-PD-1) and the personalized neoantigen vaccine NEO-PV-01⁴² (see Table S6). Epitopes incorporated into this vaccine were identified from each patient's tumor RNA sequence and whole exome sequencing as previously described.⁴² These patients were specifically selected because they exhibited *ex vivo* CD4⁺ T cell responses based on our previously published data.⁴² To verify MHCII allele restriction, previously identified reactive epitopes were assayed for binding using the above-described FP assay (Table S7). Using MHCII tetramers, neoantigen-specific CD4⁺ T cell populations were detected from patients across all three indications (Figures 4A, S6A, and S6B). These responses were only detectable post-vaccination, and neoantigen-specific CD4⁺ T cell populations were detectable as late as 76 weeks post-vaccination (Figure 4B), demonstrating that the MHCII platform can assess the durability of low-frequency antigen-specific memory CD4⁺ T cell populations.

To characterize these neoantigen-specific CD4⁺ T cells, we sorted three of the six MHCII tetramer-positive responses identified in patient L7 for single-cell sequencing analyses. The protein antigen component of the Cellular Indexing of Transcriptomes and Epitopes sequencing (CITE-seq⁴⁴) platform was used

to define a total of 10 different CD4⁺ T cell-specific subsets based on surface marker expression (Figures 4C, 4D, and S6C-S6E). All three neoantigen-specific CD4⁺ T cell populations were identified in the memory compartment (as defined by CD45RO surface expression) and were predominantly of a Th1 phenotype based on surface expression of CXCR3 (Figures 4C, 4D, S6D, and S6E). While all three neoantigen-specific populations generally clustered together (Figures 4C and S6C), some differences between populations were observed, such as the presence of a T regulatory-like subset (based on co-expression of CD39 and CD25⁴⁵) among ASP0043-DR12-reactive CD4⁺ T cells⁴² (Figures 4D, S6D, and S6E). We further assessed these L7 neoantigen-specific CD4⁺ T cells using single-cell V(D)J sequencing and found them to be clonally expanded, indicative of an immunogenic response (Figure 4E). The top 10 antigen-specific TCR sequences comprised ≥25% of all sorted tetramer-positive clones, compared with 100 top TCRs from the tetramer-negative CD4⁺ T cell population needed to reach the same cumulative frequency (Figure 4E). Interestingly, although the top five TCR clones for each epitope had a general Th1-like phenotype (except for the top ASP0043-DR12 clone, which was predominantly a T regulatory-like phenotype), each clone featured a slightly different Th1 phenotype despite a shared neoantigen specificity (Figures S6F and S6G). In summary, we applied our MHCII platform to identify and quantify multiple personal neoantigen-specific CD4⁺ T cell responses across multiple cancer indications, and combined with high-dimensional, multimodal phenotypic, and sequencing technologies, we were able to deeply characterize the phenotype of these vaccine-induced neoantigen-specific CD4⁺ T cells.

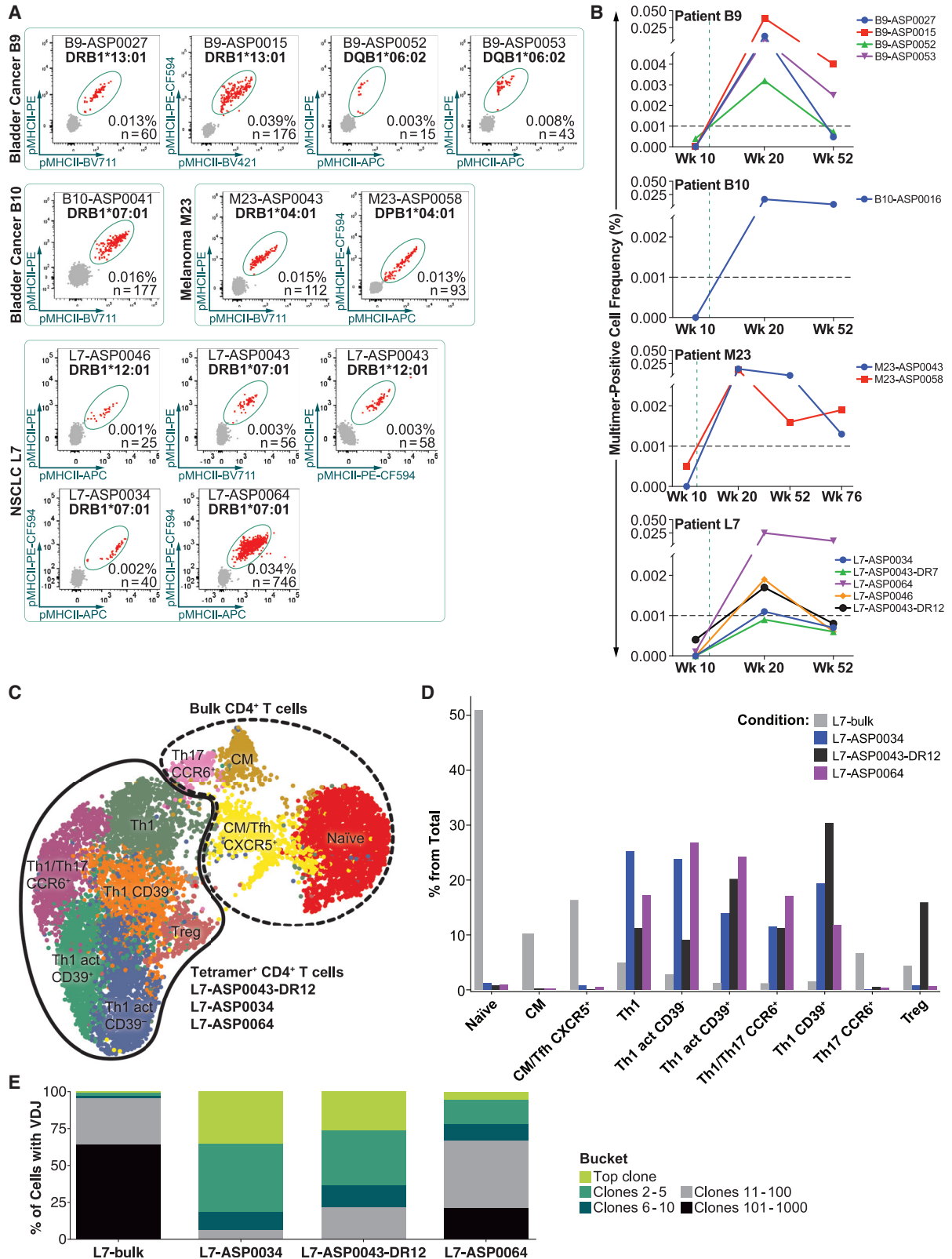
DISCUSSION

The importance of antigen-specific CD4⁺ T cells as active drivers of the immune response, particularly in the control of metastatic cancers and infectious diseases, has been studied.^{1,4} However, *ex vivo* cellular characterization has been historically challenging due to their low-frequency, low-affinity pMHCII:TCR interactions,^{31,32} and lack of robust detection approaches. Higher valency reagents^{46,47} and CD4-affinity enhanced MHCII molecules^{48,49} have been shown to improve detection of antigen-specific T cells, but universally engineering all alleles is challenging/unfeasible. To address these shortcomings, we developed a robust MHCII technology platform to identify and characterize antigen-specific CD4⁺ T cells (Figure 5). We show here the largest validated library of purified MHCII proteins, a sensitive

Figure 3. SARS-CoV-2 antigen-specific CD4⁺ T cells identified with pMHCII tetramers are predominantly effector and central memory and express markers of activation

(A) *Ex vivo* pMHCII tetramer staining of SARS-CoV-2 antigen-specific CD4⁺ T cells in five convalescent COVID-19 donor PBMCs using combinatorial coding (see Table S4 for donor information). Donors were stained with MHCII alleles loaded with SARS-CoV-2 spike (S)-, membrane (M)-, and nucleocapsid (N)-derived epitopes (see Table S5 for all alleles/epitopes tested and results). pMHCII tetramer-positive populations were gated on CD4⁺ T cells (Figure S5A) and irrelevant background tetramer staining was assessed (Figure S5B). Flow plots show tetramer-positive frequencies as a percentage of total CD4⁺ T cells and total event (n) counts observed.

(B) Phenotypic distribution of SARS-CoV-2 antigen-specific CD4⁺ T cells from donors #50833, 51861, and 53202. Effector, central memory (CM), effector memory (EM), and naive subsets were defined by CD45RA and CD62L surface expression (Figure S5C). Epitopes N₂₁₈₋₂₃₂ and S₃₅₃₋₃₅₉ (from donors #51861 and 50833, respectively) were not phenotypically characterized due to low event (n < 20) counts. Graph shows percentage of bulk or antigen-specific CD4⁺ T cells. (C) Expression of activation and suppressive markers among SARS-CoV-2 antigen-specific CD4⁺ T cells in donors #50833, 51861, and 53202. Expression shown as fold change in mean fluorescence intensity (MFI) of SARS-CoV-2 antigen-specific CD4⁺ T cells over bulk CD4⁺ T cells for each donor.



(legend on next page)

quantification assay for measuring epitope affinity and allele deconvolution, and a robust detection method using flow cytometry. Using the technology described here, we were able to detect low-frequency (0.001%) antigen-specific CD4⁺ T cells across HLA-DP, -DQ, and -DR alleles from COVID-19 convalescent subjects and metastatic cancer patients enrolled in a personalized neoantigen vaccine trial.⁴² Our technology extends and improves upon other MHCII multimer platforms that were limited by efficiency, throughput, feasibility, and scalability beyond model alleles and epitopes.

A key roadblock to deeply analyzing antigen-specific CD4⁺ T cell responses in clinical settings is generating many epitope-MHCII allele combinations. Cancers with high somatic mutations, such as melanoma, lung, and colorectal cancers, can harbor ~150 neoantigens per expressed gene in the tumor.⁵⁰ Combined with natural MHCII polymorphism,^{22–24} there is the potential for a vast number of CD4⁺ T cell neoantigen reactivities that would be impossible to analyze using current low-throughput direct refolding and epitope loading methodologies. The same case could be made for viruses, where the entirety of each foreign gene may generate many CD4⁺ T cell epitopes for evaluation. Thorough characterization of such high antigen reactivities in diverse settings thus necessitates technologies to produce many alleles, assays to identify allele restrictions, and methods for universal and high-throughput epitope loading.

Our platform allows for the rapid production of HLA-DP, -DQ, and -DR alleles representing most of the European population and with the potential to expand to any population. Commonly used peptide exchange approaches rely on small-molecule catalysts^{17,25,27,28} and/or multi-day incubation times, but these have not been demonstrated across many alleles. A UV-sensitive peptide exchange methodology has been described for some HLA-DR alleles,^{51,52} but requires the design of allele-specific degradable placeholders. Our HLA-sDM-based peptide exchange methodology overcomes these limitations by functioning as a truly universal exchange catalyst to load antigenic peptides onto any natural MHCII allele. Furthermore, HLA-sDM-mediated exchange combined with an FP assay can measure epitope/allele affinity and verify peptide loading. This approach improves upon commonly applied methodologies that involve allele-specific radioactive ligands and multiallelic mixtures to measure epitope affinity.⁵³ FP-based binding assays have been previously described for identifying MHCII epitopes, but were limited to a subset of alleles and required long incubation times.^{52,54}

The FP assay described here has been demonstrated for 28 MHCII alleles so far, is more rapid and robust than those previously described,^{53,55} and was routinely deployed to deconvolve the allele restriction of reactive epitopes for flow analysis.

Given the importance of understanding T cell responses (and their conservation among emerging viral variants⁵⁶) during the ongoing COVID-19 pandemic,⁵ we investigated the CD4⁺ T cell response to COVID-19 using our MHCII technology. Although we selected epitopes based on prediction and previously reported reactivity,^{29,30,35,36} subsequent studies using orthogonal approaches (upregulation of AIM and/or cytokines in convalescent subjects) confirm many of these epitopes (or similar regions) are immunogenic.^{57–59} Of note, the immunodominant S_{166–182} (HLA-DPB1*04:01) epitope we identified in three convalescent donors has previously been shown to be associated with circulating CD4⁺ T follicular helper cells (consistent with the upregulation of PD-1 and ICOS we observed), and was also confirmed using MHCII tetramers.³⁷ Furthermore, a recent study characterizing a CD8⁺ T cell response to the same spike region suggested suboptimal cellular priming based on their activation phenotype,^{60,61} suggesting that the S_{166–182} epitope, for which we detected upregulation of LAG3 on CD4⁺ T cells, may be a broadly detrimental T cell antigen. Given the importance of neutralizing antibodies, the crucial role that CD4⁺ T cells play in helping B cells generate durable antibodies, and the magnitude of CD4⁺ responses detected during SARS-CoV-2 infection,⁵ our MHCII technology will help deepen an understanding of the CD4⁺ compartment in COVID-19 and other infectious diseases.

The importance of CD4⁺ T cell anti-tumor responses and correlations with clinical outcomes has been previously described by us and others.^{6–9,38–43} Using our MHCII multimer platform, we detected robust and durable neoantigen-specific CD4⁺ T cell responses in metastatic cancer patients at the post-vaccination time point only, indicating the generation of *de novo* immune responses from anti-PD-1 in combination with NEO-PV-01 and consistent with our previous study.⁴² These neoantigen-specific CD4⁺ T cells have a memory, Th1-like phenotype, and potentially multiple anti-tumor functions.¹ Using our MHCII tetramers, we detected differences between these neoantigen-specific subsets, notably a T regulatory-like population in L7-ASP0043-specific CD4⁺ T cells. Although we were not able to confirm this using the expression of the T regulatory transcription factor FoxP3, the high expression of CD39 and CD25 suggests

Figure 4. In-depth pMHCII multimer characterization of neoantigen-specific CD4⁺ T cells from a personalized peptide vaccine clinical trial reveals clonal populations with memory and activated phenotypes

(A) *Ex vivo* pMHCII tetramer staining of neoantigen-specific CD4⁺ T cells from PBMCs collected post-vaccination (week 20) from cancer patients on a personalized peptide vaccine clinical trial for non-small cell lung cancer (NSCLC), melanoma, and bladder cancer⁴² (Table S6 for patient information). Wherever possible, tetramers were combi-coded³³ (Table S7 for all alleles/epitopes tested), tetramer-positive populations were gated on CD4⁺ T cells (Figure S6A), and irrelevant background tetramer staining was assessed (Figure S6B). Flow plots show tetramer-positive frequencies as a percentage of total CD4⁺ T cells and total event (n) counts observed.

(B) Durability of pMHCII tetramer-positive populations over the course of treatment. Pre-vaccination (week 10) and post-vaccination (weeks 20, 52, and 76 where applicable) PBMC samples were collected from patients and stained *ex vivo*. Vaccination with neoantigen peptides was conducted at approximately week 12 (indicated with vertical dotted line). Horizontal dotted line indicates the limit of antigen-specific CD4⁺ T cell detection using pMHCII tetramers.

(C) UMAP with clustering of bulk CD4⁺ T cells (outlined with the dotted line) and three pMHCII tetramer-positive populations from NSCLC patient L7 (outlined with the solid line), based on CITE antibodies (see key resources table for all antibodies). UMAP with overlaid unsupervised clustering defined 10 distinct populations.

(D) CD4⁺ T cell phenotypes of NSCLC patient L7 bulk and pMHCII tetramer-positive populations, based on the expression of CITE antibodies.

(E) Clonal distribution and abundance of TCRs sorted from each NSCLC patient L7 pMHCII tetramer-positive population and bulk CD4⁺ T cells.

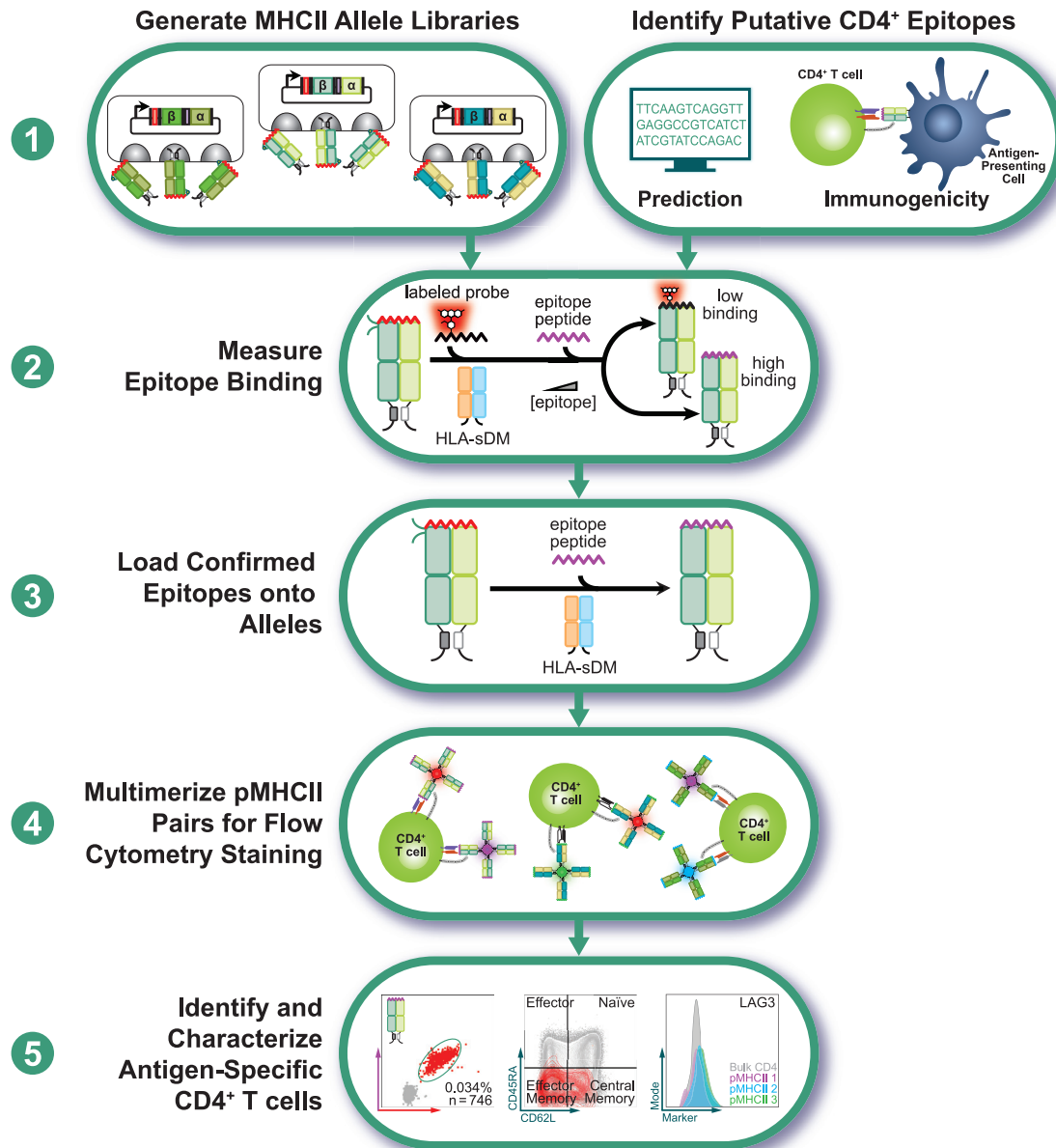


Figure 5. Strategy to investigate any potential CD4⁺ response via the pMHCII technology platform

Step 1: MHCII alleles can be purified in parallel to epitope identification (via computational prediction and/or immunogenicity screening). Step 2: Candidate epitope/allele pairs are validated using the FP assay. Step 3: Epitope peptides of interest are loaded onto MHCII via HLA-sDM to create the pMHCII antigen for staining. Step 4: pMHCII is multimerized via conjugation to fluorescent streptavidins and subsequently combi-coded to stain CD4⁺ T cells (here, three distinct antigen-specific CD4⁺ T cell populations are combi-coded, each with a unique two-color combination). Step 5: Stained antigen-specific CD4⁺ T cells can be further analyzed for expression markers through flow cytometry and/or sorted for single-cell analyses.

that this subset is likely a T regulatory population.⁴⁵ This in-depth phenotyping using our MHCII multimers can provide insights into the mechanisms and functions of CD4⁺ T cells in the context of cancer progression and treatments. Future correlations of CD4⁺ T cell phenotype with clinical outcome could demonstrate the utility of MHCII multimers as a tool for biomarker discovery to guide clinical decision making.

In summary, we describe a robust MHCII platform that can identify and characterize CD4⁺ T cells across many disease

settings. By coupling rapid allele generation, epitope prediction and validation, peptide loading, and detection, we offer a comprehensive pipeline for identifying antigen-specific CD4⁺ T cells, without relying on methods that limit the depth of *ex vivo* phenotypic characterization (Figure 5). We believe this technology can be used to provide deep and comprehensive insights into CD4⁺ T cell-mediated immunity beyond model alleles and epitopes, and beyond cancer and infectious disease settings.

Limitations of the study

Successful identification of antigen-specific CD4⁺ T cells depends on properly defining the peptide epitopes to which they are reactive, a process that usually starts with *in silico* prediction. Here, we show that once a peptide epitope is nominated for study, its allele restriction and binding affinity can be validated with an *in vitro* assay. Combinatorial coding of fluorescent pMHCII tetramers is limited by available streptavidin fluorochromes and their non-specific binding profiles to CD4⁺ T cells—future higher dimensional applications of pMHCII multimers (i.e., detecting multiple antigen specificities per sample) will depend on either the introduction of new fluorochromes or coupling to next generation nucleic acid sequencing technologies (e.g., DNA barcodes).

STAR★METHODS

Detailed methods are provided in the online version of this paper and include the following:

- **KEY RESOURCES TABLE**
- **RESOURCE AVAILABILITY**
 - Lead contact
 - Materials availability
 - Data and code availability
- **EXPERIMENTAL MODEL AND SUBJECT DETAILS**
 - Healthy donor and patient samples
- **METHOD DETAILS**
 - Soluble MHCII protein construct design, expression, and purification
 - Soluble HLA-DM construct design, expression, and purification
 - MHCII FITC-peptide probe synthesis and purification
 - Fluorescence polarization (FP) assay
 - Immunoprecipitation for epitope loading efficiency
 - Analytical SEC of MHCII protein stability
 - Epitope loading for multimer analysis
 - MHCII multimerization, staining, and activation panel
 - Flow cytometry analysis
 - T cell induction in healthy donor samples
 - Cell sorting and CITEseq antibody labeling
 - Single-cell TCR and surface epitope sequencing
- **QUANTIFICATION AND STATISTICAL ANALYSIS**
 - Single cell CITE/TCR analysis
 - Statistical analysis

SUPPLEMENTAL INFORMATION

Supplemental information can be found online at <https://doi.org/10.1016/j.crmeth.2022.100388>.

ACKNOWLEDGMENTS

We thank Marit van Buuren and Terri Addona for their insightful comments, suggestions, and assistance during manuscript preparation. We thank April Lamb, Jennifer Tepper, Melissa Moles, Amy Wanamaker, and Zakaria Khondker for their hard work on the clinical data from the NEO-PV-01 studies. We thank all BioNTech US employees for their dedication and support in this study. We thank John Welle of Acumen Medical Communications for graphic design support. Finally, we thank Andrew Finlayson, Kelledy Man-

son, Amy Greenstein, Mark De Mario, Rana Sawaya, Chris McAndrew, and Sanjukta Ghosh for their guidance and critical review of materials prior to submission.

AUTHOR CONTRIBUTIONS

R.V., V.K., M.E.B., and J.R.S. conceived and designed the project. R.V., V.K., B.K., G.M., and J.H.S. performed experiments and analyzed data. K.E. and A.P. performed analysis on single-cell experiments. J.M., D.K., and J.D. synthesized and purified peptides for tetramer generation and experiments. D.H., M.K., and A.P. provided bioinformatics support and epitope predictions. L.S., R.B.G., M.E.B., and J.R.S. discussed results and supervised the study. R.V., V.K., M.E.B., and J.R.S. wrote the manuscript. All authors read, revised, and approved the manuscript.

DECLARATION OF INTERESTS

R.V., V.K., B.K., G.M., K.E., J.M., D.K., J.H.S., D.H., M.K., A.P., J.D., L.S., R.B.G., M.E.B., and J.R.S., are all current or former employees and/or equity holders of BioNTech SE. D.H. is a current employee of Prime Medicine, Inc., and L.S. is a current employee of Repertoire Immune Medicines, Inc. R.B.G. is a member of the board of directors at Alkermes PLC, Infinity Pharmaceuticals, and Zai Lab, as well as a member of the scientific advisory board at Leap Therapeutics. Patents have been filed relating to this work.

INCLUSION AND DIVERSITY

We support inclusive, diverse, and equitable conduct of research.

Received: June 29, 2022

Revised: November 8, 2022

Accepted: December 20, 2022

Published: January 13, 2023

REFERENCES

1. Tay, R.E., Richardson, E.K., and Toh, H.C. (2021). Revisiting the role of CD4⁺ T cells in cancer immunotherapy—new insights into old paradigms. *Cancer Gene Ther.* 28, 5–17. <https://doi.org/10.1038/s41417-020-0183-x>.
2. Geginat, J., Paroni, M., Maglie, S., Alfen, J.S., Kastirr, I., Gruarin, P., De Simone, M., Pagani, M., and Abrignani, S. (2014). Plasticity of human CD4 T cell subsets. *Front. Immunol.* 5, 630. <https://doi.org/10.3389/fimmu.2014.00630>.
3. Jenkins, M.K., Khoruts, A., Ingulli, E., Mueller, D.L., McSorley, S.J., Reinhardt, R.L., Itano, A., and Pape, K.A. (2001). In vivo activation of antigen-specific CD4 T cells. *Annu. Rev. Immunol.* 19, 23–45. <https://doi.org/10.1146/annurev.immunol.19.1.23>.
4. Swain, S.L., McKinstry, K.K., and Strutt, T.M. (2012). Expanding roles for CD4⁺ T cells in immunity to viruses. *Nat. Rev. Immunol.* 12, 136–148. <https://doi.org/10.1038/nri3152>.
5. Moss, P. (2022). The T cell immune response against SARS-CoV-2. *Nat. Immunol.* 23, 186–193. <https://doi.org/10.1038/s41590-021-01122-w>.
6. Linnemann, C., van Buuren, M.M., Bies, L., Verdegaal, E.M.E., Schotte, R., Calis, J.J.A., Behjati, S., Velds, A., Hilkmann, H., Atmioui, D.E., et al. (2015). High-throughput epitope discovery reveals frequent recognition of neo-antigens by CD4⁺ T cells in human melanoma. *Nat. Med.* 21, 81–85. <https://doi.org/10.1038/nm.3773>.
7. Kreiter, S., Vormehr, M., van de Roemer, N., Diken, M., Löwer, M., Diekmann, J., Boegel, S., Schrörs, B., Vascotto, F., Castle, J.C., et al. (2015). Mutant MHC class II epitopes drive therapeutic immune responses to cancer. *Nature* 520, 692–696. <https://doi.org/10.1038/nature14426>.

8. Poncette, L., Bluhm, J., and Blankenstein, T. (2022). The role of CD4 T cells in rejection of solid tumors. *Curr. Opin. Immunol.* *74*, 18–24. <https://doi.org/10.1016/j.coi.2021.09.005>.
9. Alspach, E., Lussier, D.M., Miceli, A.P., Kizhvatov, I., DuPage, M., Luoma, A.M., Meng, W., Lichti, C.F., Esaulova, E., Vomund, A.N., et al. (2019). MHC-II neoantigens shape tumour immunity and response to immunotherapy. *Nature* *574*, 696–701. <https://doi.org/10.1038/s41586-019-1671-8>.
10. Reiss, S., Baxter, A.E., Cirelli, K.M., Dan, J.M., Morou, A., Daigneault, A., Brassard, N., Silvestri, G., Routy, J.-P., Havenar-Daughton, C., et al. (2017). Comparative analysis of activation induced marker (AIM) assays for sensitive identification of antigen-specific CD4 T cells. *PLoS One* *12*, e0186998. <https://doi.org/10.1371/journal.pone.0186998>.
11. Campbell, J.D.M. (2003). Detection and enrichment of antigen-specific CD4+ and CD8+ T cells based on cytokine secretion. *Methods* *31*, 150–159. [https://doi.org/10.1016/S1046-2023\(03\)00125-7](https://doi.org/10.1016/S1046-2023(03)00125-7).
12. Rudensky, A., Preston-Hurlburt, P., Hong, S.C., Barlow, A., and Janeway, C.A. (1991). Sequence analysis of peptides bound to MHC class II molecules. *Nature* *353*, 622–627. <https://doi.org/10.1038/353622a0>.
13. Cameron, T.O., Norris, P.J., Patel, A., Moulon, C., Rosenberg, E.S., Mellins, E.D., Wedderburn, L.R., and Stern, L.J. (2002). Labeling antigen-specific CD4(+) T cells with class II MHC oligomers. *J. Immunol. Methods* *268*, 51–69. [https://doi.org/10.1016/S0022-1759\(02\)00200-4](https://doi.org/10.1016/S0022-1759(02)00200-4).
14. Stöckel, J., Meinel, E., Hahnel, C., Malotka, J., Seitz, R., Drexler, K., Wekerle, H., and Dornmair, K. (1994). Refolding of human class II major histocompatibility complex molecules isolated from *Escherichia coli*. Assembly of peptide-free heterodimers and increased refolding-yield in the presence of antigenic peptide. *J. Biol. Chem.* *269*, 29571–29578. [https://doi.org/10.1016/S0021-9258\(18\)43918-X](https://doi.org/10.1016/S0021-9258(18)43918-X).
15. Kozono, H., White, J., Clements, J., Marrack, P., and Kappler, J. (1994). Production of soluble MHC class II proteins with covalently bound single peptides. *Nature* *369*, 151–154. <https://doi.org/10.1038/369151a0>.
16. Kotzin, B.L., Falta, M.T., Crawford, F., Rosloniec, E.F., Bill, J., Marrack, P., and Kappler, J. (2000). Use of soluble peptide-DR4 tetramers to detect synovial T cells specific for cartilage antigens in patients with rheumatoid arthritis. *Proc. Natl. Acad. Sci. USA* *97*, 291–296. <https://doi.org/10.1073/pnas.97.1.291>.
17. Day, C.L., Seth, N.P., Lucas, M., Appel, H., Gauthier, L., Lauer, G.M., Robbins, G.K., Szczepiorkowski, Z.M., Casson, D.R., Chung, R.T., et al. (2003). Ex vivo analysis of human memory CD4 T cells specific for hepatitis C virus using MHC class II tetramers. *J. Clin. Invest.* *112*, 831–842. <https://doi.org/10.1172/JCI200318509>.
18. Natarajan, S.K., Assadi, M., and Sadegh-Nasseri, S. (1999). Stable peptide binding to MHC class II molecule is rapid and is determined by a receptive conformation shaped by prior association with low affinity peptides. *J. Immunol.* *162*, 4030–4036.
19. Rupp, B., Günther, S., Makhmou, T., Schlundt, A., Dickhaut, K., Gupta, S., Choudhary, I., Wiesmüller, K.H., Jung, G., Freund, C., et al. (2011). Characterization of structural features controlling the receptiveness of empty class II MHC molecules. *PLoS One* *6*, e18662. <https://doi.org/10.1371/journal.pone.0018662>.
20. Rock, K.L., Reits, E., and Neefjes, J. (2016). Present yourself! By MHC class I and MHC class II molecules. *Trends Immunol.* *37*, 724–737. <https://doi.org/10.1016/j.it.2016.08.010>.
21. Roche, P.A., and Furuta, K. (2015). The ins and outs of MHC class II-mediated antigen processing and presentation. *Nat. Rev. Immunol.* *15*, 203–216. <https://doi.org/10.1038/nri3818>.
22. Gragert, L., Madbouly, A., Freeman, J., and Maiers, M. (2013). Six-locus high resolution HLA haplotype frequencies derived from mixed-resolution DNA typing for the entire US donor registry. *Hum. Immunol.* *74*, 1313–1320. <https://doi.org/10.1016/j.humimm.2013.06.025>.
23. Hollenbach, J.A., Madbouly, A., Gragert, L., Vierra-Green, C., Fleisch, S., Spellman, S., Begovich, A., Noreen, H., Trachtenberg, E., Williams, T., et al. (2012). A combined DPA1-DPB1 amino acid epitope is the primary unit of selection on the HLA-DP heterodimer. *Immunogenetics* *64*, 559–569. <https://doi.org/10.1007/s00251-012-0615-3>.
24. Klitz, W., Maiers, M., Spellman, S., Baxter-Lowe, L.A., Schmeckpeper, B., Williams, T.M., and Fernandez-Viña, M. (2003). New HLA haplotype frequency reference standards: high-resolution and large sample typing of HLA DR-DQ haplotypes in a sample of European Americans. *Tissue Antigens* *62*, 296–307. <https://doi.org/10.1034/j.1399-0039.2003.00103.x>.
25. Chou, C.-L., Mirshahidi, S., Su, K.W., Kim, A., Narayan, K., Khoruzhenko, S., Xu, M., and Sadegh-Nasseri, S. (2008). Short peptide sequences mimic HLA-DM functions. *Mol. Immunol.* *45*, 1935–1943. <https://doi.org/10.1016/j.molimm.2007.10.033>.
26. Call, M.J., Xing, X., Cuny, G.D., Seth, N.P., Altmann, D.M., Fugger, L., Krogsgaard, M., Stein, R.L., and Wucherpfennig, K.W. (2009). In vivo enhancement of peptide display by MHC class II molecules with small molecule catalysts of peptide exchange. *J. Immunol.* *182*, 6342–6352. <https://doi.org/10.4049/jimmunol.0803464>.
27. Novak, E.J., Liu, A.W., Nepom, G.T., and Kwok, W.W. (1999). MHC class II tetramers identify peptide-specific human CD4+ T cells proliferating in response to influenza A antigen. *J. Clin. Invest.* *104*, R63–R67.
28. Kwok, W.W., Liu, A.W., Novak, E.J., Gebe, J.A., Ettinger, R.A., Nepom, G.T., Raymond, S.N., and Koelle, D.M. (2000). HLA-DQ tetramers identify epitope-specific T cells in peripheral blood of herpes simplex virus type 2-infected individuals: direct detection of immunodominant antigen-responsive cells. *J. Immunol.* *164*, 4244–4249. <https://doi.org/10.4049/jimmunol.164.8.4244>.
29. Abelin, J.G., Harjanto, D., Malloy, M., Suri, P., Colson, T., Goulding, S.P., Creech, A.L., Serrano, L.R., Nasir, G., Nasrullah, Y., et al. (2019). Defining HLA-II ligand processing and binding rules with mass spectrometry enhances cancer epitope prediction. *Immunity* *51*, 766–779.e17. <https://doi.org/10.1016/j.immuni.2019.08.012>.
30. Poran, A., Harjanto, D., Malloy, M., Arieta, C.M., Rothenberg, D.A., Lenkala, D., van Buuren, M.M., Addona, T.A., Rooney, M.S., Srinivasan, L., and Gaynor, R.B. (2020). Sequence-based prediction of SARS-CoV-2 vaccine targets using a mass spectrometry-based bioinformatics predictor identifies immunogenic T cell epitopes. *Genome Med.* *12*, 70. <https://doi.org/10.1186/s13073-020-00767-w>.
31. Stone, J.D., Chervin, A.S., and Kranz, D.M. (2009). T-cell receptor binding affinities and kinetics: impact on T-cell activity and specificity. *Immunology* *126*, 165–176. <https://doi.org/10.1111/j.1365-2567.2008.03015.x>.
32. van der Merwe, P.A., and Davis, S.J. (2003). Molecular interactions mediating T cell antigen recognition. *Annu. Rev. Immunol.* *21*, 659–684. <https://doi.org/10.1146/annurev.immunol.21.120601.141036>.
33. Hadrup, S.R., Bakker, A.H., Shu, C.J., Andersen, R.S., van Veluw, J., Hombrink, P., Castermans, E., Thor Straten, P., Blank, C., Haanen, J.B., et al. (2009). Parallel detection of antigen-specific T-cell responses by multidimensional encoding of MHC multimers. *Nat. Methods* *6*, 520–526. <https://doi.org/10.1038/nmeth.1345>.
34. Uchtenhagen, H., Rims, C., Blahnik, G., Chow, I.-T., Kwok, W.W., Buckner, J.H., and James, E.A. (2016). Efficient ex vivo analysis of CD4+ T-cell responses using combinatorial HLA class II tetramer staining. *Nat. Commun.* *7*, 12614. <https://doi.org/10.1038/ncomms12614>.
35. Tarke, A., Sidney, J., Kidd, C.K., Dan, J.M., Ramirez, S.I., Yu, E.D., Mateus, J., da Silva Antunes, R., Moore, E., Rubio, P., et al. (2021). Comprehensive analysis of T cell immunodominance and immunoprevalence of SARS-CoV-2 epitopes in COVID-19 cases. *Cell Rep. Med.* *2*, 100204. <https://doi.org/10.1016/j.xcrm.2021.100204>.
36. Tarke, A., Sidney, J., Methot, N., Yu, E.D., Zhang, Y., Dan, J.M., Goodwin, B., Rubio, P., Sutherland, A., Wang, E., et al. (2021). Impact of SARS-CoV-2 variants on the total CD4+ and CD8+ T cell reactivity in infected or vaccinated individuals. *Cell Rep. Med.* *2*, 100355. <https://doi.org/10.1016/j.xcrm.2021.100355>.

37. Mudd, P.A., Minervina, A.A., Pogorelyy, M.V., Turner, J.S., Kim, W., Kalaidina, E., Petersen, J., Schmitz, A.J., Lei, T., Haile, A., et al. (2022). SARS-CoV-2 mRNA vaccination elicits a robust and persistent T follicular helper cell response in humans. *Cell* 185, 603–613.e15. <https://doi.org/10.1016/j.cell.2021.12.026>.
38. Oh, D.Y., and Fong, L. (2021). Cytotoxic CD4+ T cells in cancer: expanding the immune effector toolbox. *Immunity* 54, 2701–2711. <https://doi.org/10.1016/j.immuni.2021.11.015>.
39. Martens, A., Wistuba-Hamprecht, K., Yuan, J., Postow, M.A., Wong, P., Capone, M., Madonna, G., Khammari, A., Schilling, B., Sucker, A., et al. (2016). Increases in absolute lymphocytes and circulating CD4+ and CD8+ T cells are associated with positive clinical outcome of melanoma patients treated with ipilimumab. *Clin. Cancer Res.* 22, 4848–4858. <https://doi.org/10.1158/1078-0432.CCR-16-0249>.
40. Kagamu, H., Kitano, S., Yamaguchi, O., Yoshimura, K., Horimoto, K., Kitazawa, M., Fukui, K., Shiono, A., Mouri, A., Nishihara, F., et al. (2020). CD4+ T-cell immunity in the peripheral blood correlates with response to anti-PD-1 therapy. *Cancer Immunol. Res.* 8, 334–344. <https://doi.org/10.1158/2326-6066.CIR-19-0574>.
41. Kwek, S.S., Lewis, J., Zhang, L., Weinberg, V., Greaney, S.K., Harzstark, A.L., Lin, A.M., Ryan, C.J., Small, E.J., and Fong, L. (2015). Preexisting levels of CD4 T cells expressing PD-1 are related to overall survival in prostate cancer patients treated with ipilimumab. *Cancer Immunol. Res.* 3, 1008–1016. <https://doi.org/10.1158/2326-6066.CIR-14-0227>.
42. Ott, P.A., Hu-Lieskovan, S., Chmielowski, B., Govindan, R., Naing, A., Bhardwaj, N., Margolin, K., Awad, M.M., Hellmann, M.D., Lin, J.J., et al. (2020). A phase Ib trial of personalized neoantigen therapy Plus anti-PD-1 in patients with advanced melanoma, non-small cell lung cancer, or bladder cancer. *Cell* 183, 347–362.e24. <https://doi.org/10.1016/j.cell.2020.08.053>.
43. Sahin, U., Derhovanessian, E., Miller, M., Kloke, B.-P., Simon, P., Löwer, M., Bukur, V., Tadmor, A.D., Luxemburger, U., Schrörs, B., et al. (2017). Personalized RNA mutanome vaccines mobilize poly-specific therapeutic immunity against cancer. *Nature* 547, 222–226. <https://doi.org/10.1038/nature23003>.
44. Stoeckius, M., Hafemeister, C., Stephenson, W., Houck-Loomis, B., Chattopadhyay, P.K., Swerdlow, H., Satija, R., and Smibert, P. (2017). Simultaneous epitope and transcriptome measurement in single cells. *Nat. Methods* 14, 865–868. <https://doi.org/10.1038/nmeth.4380>.
45. Borsellino, G., Kleinewietfeld, M., Di Mitri, D., Sternjak, A., Diamantini, A., Giometto, R., Höpner, S., Centonze, D., Bernardi, G., Dell'Acqua, M.L., et al. (2007). Expression of ectonucleotidase CD39 by Foxp3+ Treg cells: hydrolysis of extracellular ATP and immune suppression. *Blood* 110, 1225–1232. <https://doi.org/10.1182/blood-2006-12-064527>.
46. Dolton, G., Zervoudi, E., Rius, C., Wall, A., Thomas, H.L., Fuller, A., Yeo, L., Legut, M., Wheeler, S., Attaf, M., et al. (2018). Optimized peptide–MHC multimer protocols for detection and isolation of autoimmune T-cells. *Front. Immunol.* 9, 1378. <https://doi.org/10.3389/fimmu.2018.01378>.
47. Massilamany, C., Upadhyaya, B., Gangaplara, A., Kuszynski, C., and Reddy, J. (2011). Detection of autoreactive CD4 T cells using major histocompatibility complex class II dextramers. *BMC Immunol.* 12, 40. <https://doi.org/10.1186/1471-2172-12-40>.
48. Sugata, K., Matsunaga, Y., Yamashita, Y., Nakatsugawa, M., Guo, T., Habelian, L., Ohashi, Y., Saso, K., Rahman, M.A., Anczurowski, M., et al. (2021). Affinity-matured HLA class II dimers for robust staining of antigen-specific CD4+ T cells. *Nat. Biotechnol.* 39, 958–967. <https://doi.org/10.1038/s41587-021-00836-4>.
49. Dileepan, T., Malhotra, D., Kotov, D.I., Kolawole, E.M., Krueger, P.D., Evavold, B.D., and Jenkins, M.K. (2021). MHC class II tetramers engineered for enhanced binding to CD4 improve detection of antigen-specific T cells. *Nat. Biotechnol.* 39, 943–948. <https://doi.org/10.1038/s41587-021-00893-9>.
50. Schumacher, T.N., and Schreiber, R.D. (2015). Neoantigens in cancer immunotherapy. *Science* 348, 69–74. <https://doi.org/10.1126/science.aaa4971>.
51. Negroni, M.P., and Stern, L.J. (2018). The N-terminal region of photocleavable peptides that bind HLA-DR1 determines the kinetics of fragment release. *PLoS One* 13, e0199704. <https://doi.org/10.1371/journal.pone.0199704>.
52. Grotenberg, G.M., Nicholson, M.J., Fowler, K.D., Wilbuer, K., Octavio, L., Yang, M., Chakraborty, A.K., Ploegh, H.L., and Wucherpfennig, K.W. (2007). Empty class II major histocompatibility complex created by peptide photolysis establishes the role of DM in peptide association. *J. Biol. Chem.* 282, 21425–21436. <https://doi.org/10.1074/jbc.M702844200>.
53. Sidney, J., Southwood, S., Moore, C., Oseroff, C., Pinilla, C., Grey, H.M., and Sette, A. (2013). Measurement of MHC/Peptide interactions by gel filtration or monoclonal antibody capture. *E.C. John, ed.* 18, Unit-18.3. <https://doi.org/10.1002/0471142735.im1803s100>.
54. Yin, L., and Stern, L.J. (2014). Measurement of peptide binding to MHC class II molecules by fluorescence polarization. *Curr. Protoc. Immunol.* 106, 5.10.1–5.10.12. <https://doi.org/10.1002/0471142735.im0510s106>.
55. Justesen, S., Harndahl, M., Lamberth, K., Nielsen, L.-L.B., and Buus, S. (2009). Functional recombinant MHC class II molecules and high-throughput peptide-binding assays. *Immunome Res.* 5, 2. <https://doi.org/10.1186/1745-7580-5-2>.
56. Tarke, A., Coelho, C.H., Zhang, Z., Dan, J.M., Yu, E.D., Methot, N., Bloom, N.I., Goodwin, B., Phillips, E., Mallal, S., et al. (2022). SARS-CoV-2 vaccination induces immunological T cell memory able to cross-recognize variants from Alpha to Omicron. *Cell* 185, 847–859.e11. <https://doi.org/10.1016/j.cell.2022.01.015>.
57. Heide, J., Schulte, S., Kohsar, M., Brehm, T.T., Herrmann, M., Karsten, H., Marget, M., Peine, S., Johansson, A.M., Sette, A., et al. (2021). Broadly directed SARS-CoV-2-specific CD4+ T cell response includes frequently detected peptide specificities within the membrane and nucleoprotein in patients with acute and resolved COVID-19. *PLoS Pathog.* 17, e1009842. <https://doi.org/10.1371/journal.ppat.1009842>.
58. Nelde, A., Bilich, T., Heitmann, J.S., Maringer, Y., Salih, H.R., Roerden, M., Lübke, M., Bauer, J., Rieth, J., Wacker, M., et al. (2021). SARS-CoV-2-derived peptides define heterologous and COVID-19-induced T cell recognition. *Nat. Immunol.* 22, 74–85. <https://doi.org/10.1038/s41590-020-00808-x>.
59. Verhagen, J., van der Meijden, E.D., Lang, V., Kremer, A.E., Völkl, S., Mackensen, A., Aigner, M., and Kremer, A.N. (2021). Human CD4+ T cells specific for dominant epitopes of SARS-CoV-2 Spike and Nucleocapsid proteins with therapeutic potential. *Clin. Exp. Immunol.* 205, 363–378. <https://doi.org/10.1111/cei.13627>.
60. Habel, J.R., Nguyen, T.H.O., van de Sandt, C.E., Juno, J.A., Chaurasia, P., Wragg, K., Koutsakos, M., Hensen, L., Jia, X., Chua, B., et al. (2020). Sub-optimal SARS-CoV-2-specific CD8+ T cell response associated with the prominent HLA-A*02:01 phenotype. *Proc. Natl. Acad. Sci. USA* 117, 24384–24391. <https://doi.org/10.1073/pnas.2015486117>.
61. Nguyen, T.H.O., Rowntree, L.C., Petersen, J., Chua, B.Y., Hensen, L., Kedzierski, L., van de Sandt, C.E., Chaurasia, P., Tan, H.-X., Habel, J.R., et al. (2021). CD8+ T cells specific for an immunodominant SARS-CoV-2 nucleocapsid epitope display high naive precursor frequency and TCR promiscuity. *Immunity* 54, 1066–1082.e5. <https://doi.org/10.1016/j.immuni.2021.04.009>.
62. Barash, S., Wang, W., and Shi, Y. (2002). Human secretory signal peptide description by hidden Markov model and generation of a strong artificial signal peptide for secreted protein expression. *Biochem. Biophys. Res. Commun.* 294, 835–842. [https://doi.org/10.1016/S0006-291X\(02\)00566-1](https://doi.org/10.1016/S0006-291X(02)00566-1).
63. Güler-Gane, G., Kidd, S., Sridharan, S., Vaughan, T.J., Wilkinson, T.C.I., and Tigue, N.J. (2016). Overcoming the refractory expression of secreted recombinant proteins in mammalian cells through modification of the

- signal peptide and adjacent amino acids. *PLoS One* 11, e0155340. <https://doi.org/10.1371/journal.pone.0155340>.
64. Stuart, T., Butler, A., Hoffman, P., Hafemeister, C., Papalexi, E., Mauck, W.M., Hao, Y., Stoeckius, M., Smibert, P., and Satija, R. (2019). Comprehensive integration of single-cell data. *Cell* 177, 1888–1902.e21. <https://doi.org/10.1016/j.cell.2019.05.031>.
65. Gu, Z., Eils, R., and Schlesner, M. (2016). Complex heatmaps reveal patterns and correlations in multidimensional genomic data. *Bioinformatics* 32, 2847–2849. <https://doi.org/10.1093/bioinformatics/btw313>.
66. Signorell, A., Aho, K., Alfons, A., Anderegg, N., Aragon, T., Arachchige, C., Arppe, A., Baddeley, A., Barton, K., and Bolker, B. (2021). DescTools: Tools for Descriptive Statistics. R package version 0.99.44. <https://cran.r-project.org/web/packages/DescTools/index.html>.
67. Wickham, H., Chang, H., Henry, L., Pedersen, T.L., Takahashi, K., Wilke, C., Woo, K., Yutani, H., and Dunnington, D. (2016). *ggplot2* (Springer-Verlag New York).

STAR★METHODS

KEY RESOURCES TABLE

REAGENT or RESOURCE	SOURCE	IDENTIFIER
Antibodies		
FITC monoclonal antibody	Thermo Fisher Scientific	Cat# 31242; RRID: AB_429692
CD197 (CCR7)-FITC	BioLegend	Cat# 353216; RRID:AB_10916386
CD3-BUV805	BD Biosciences	Cat# 612893; RRID:AB_2870181
CD4-FITC	BD Biosciences	Cat# 347413; RRID:AB_400297
CD3-FITC	BioLegend	Cat# 300306; RRID:AB_314042
CD4-BUV395	BD Biosciences	Cat# 563550; RRID:AB_2738273
CD8-APC-H7	BD Biosciences	Cat# 561423; RRID:AB_10682894
CD8-Alexa Fluor 700	BioLegend	Cat# 344724; RRID:AB_2562790
CD8-BUV496	BD Biosciences	Cat# 741199; RRID:AB_2870759
CD16-Alexa Fluor 700	BD Biosciences	Cat# 557920; RRID:AB_396941
CD14-Alexa Fluor 700	BD Biosciences	Cat# 557923; RRID:AB_396944
CD19-APC-H7	BD Biosciences	Cat# 560177; RRID:AB_1645470
CD19-Alexa Fluor 700	BD Biosciences	Cat# 557921; RRID:AB_396942
CD27-BV605	BioLegend	Cat# 302830; RRID:AB_2561450
CD45RA-Alexa Fluor 700	BD Biosciences	Cat# 560673; RRID:AB_1727496
CD45RO-PerCP-Cy5.5	BD Biosciences	Cat# 560607; RRID:AB_1727500
CD62L-FITC	BD Biosciences	Cat# 555543; RRID:AB_395927
CD69-PE-Cy7	BD Biosciences	Cat# 557745; RRID:AB_396851
CD137 (4-1BB)-BV650	BD Biosciences	Cat# 564092; RRID:AB_2738586
CD137 (4-1BB)-PE-Cy5	BD Biosciences	Cat# 551137; RRID:AB_394067
CD278 (ICOS)-BV421	BD Biosciences	Cat# 562901; RRID:AB_2737878
CD278 (ICOS)-BV786	BD Biosciences	Cat# 741017; RRID:AB_2740638
CD223 (LAG-3)-BV786	BD Biosciences	Cat# 744727; RRID:AB_2742438
LIVE/DEAD Fixable Near-IR Dead Cell Stain Kit	ThermoFisher	Cat # L10119
CD279 (PD-1)-PE-eFluor 610	eBioscience	Cat # 61-2799-42
CD279 (PD-1)-BV650	BD Biosciences	Cat# 564104; RRID:AB_2738595
CD366 (Tim-3)-BV510	BioLegend	Cat# 345030; RRID:AB_2565831
TotalSeq(TM)-C0148 anti-human CD197 (CCR7)	BioLegend	Cat# 353251; RRID:AB_2800943
TotalSeq(TM)-C0085 anti-human CD25	BioLegend	Cat# 302649; RRID:AB_2800745
TotalSeq(TM)-C0154 anti-human CD27	BioLegend	Cat# 302853; RRID:AB_2800747
TotalSeq(TM)-C0171 anti-human/mouse/rat CD278 (ICOS)	BioLegend	Cat# 313553; RRID:AB_2800823
TotalSeq(TM)-C0176 anti-human CD39	BioLegend	Cat# 328237; RRID:AB_2800853
TotalSeq(TM)-C0063 anti-human CD45RA	BioLegend	Cat# 304163; RRID:AB_2800764
TotalSeq(TM)-C0087 anti-human CD45RO	BioLegend	Cat# 304259; RRID:AB_2800766
TotalSeq(TM)-C0147 anti-human CD62L	BioLegend	Cat# 304851; RRID:AB_2800770
TotalSeq(TM)-C0390 anti-human CD127 (IL-7Ralpha)	BioLegend	Cat# 351356; RRID:AB_2800937
TotalSeq(TM)-C0396 anti-human CD26	BioLegend	Cat# 302722; RRID:AB_2810435
TotalSeq(TM)-C0088 anti-human CD279 (PD-1)	BioLegend	Cat# 329963; RRID:AB_2800862

(Continued on next page)

Continued

REAGENT or RESOURCE	SOURCE	IDENTIFIER
TotalSeq(TM)-C0146 anti-human CD69	BioLegend	Cat# 310951; RRID:AB_2800810
TotalSeq(TM)-C0089 anti-human TIGIT (VSTM3)	BioLegend	Cat# 372729; RRID:AB_2801021
TotalSeq(TM)-C0386 anti-human CD28	BioLegend	Cat# 302963; RRID:AB_2800751
TotalSeq(TM)-C0144 anti-human CD185	BioLegend	Cat# 356939; RRID:AB_2800968
TotalSeq(TM)-C0143 anti-human CD196 (CCR6)	BioLegend	Cat# 353440; RRID:AB_2810563
TotalSeq(TM)-C0140 anti-human CD183 (CXCR3)	BioLegend	Cat# 353747; RRID:AB_2800949
TotalSeq(TM)-C0156 anti-human CD95 (Fas)	BioLegend	Cat# 305651; RRID:AB_2800787
TotalSeq(TM)-C0410 anti-human CD38	BioLegend	Cat# 356637; RRID:AB_2820007
Streptavidin-PE	Agilent	Cat # PJRS25-1
Streptavidin-PE	BioLegend	Cat # 405204
Streptavidin-APC	Agilent	Cat # PJ27S
Streptavidin-APC	BioLegend	Cat # 405207
Streptavidin-BV711	BD Biosciences	Cat# 563262; RRID:AB_2869478
Streptavidin-PE-CF594	BD Biosciences	Cat# 562284; RRID:AB_11154598
Streptavidin-BV421	BioLegend	Cat # 405225
Klickmer-PE	Immudex	Cat # DX01-PE
Biological samples		
Patient PBMCs from NT-001 trial	NCT02897765	N/A
Healthy Donor PBMCs	StemExpress	Cat # LE010F
COVID-19 PBMCs	Precision for Medicine	Lot# 53207, 53208, 51861, 53202, 50833
Chemicals, peptides, and recombinant proteins		
Thrombin, Bovine	Millipore Sigma	Cat # 605157-1KU
MHC class II alleles	This manuscript	Table S1
HLA-DM	This manuscript	N/A
BirA	This manuscript	N/A
Gammabind Plus Sepharose	Cytiva	Cat # 17088602
Dasatinib	Sigma-Aldrich	Cat # CDS023389
Benzonase	Millipore Sigma	Cat # 70746
d-biotin solution	AVIDITY	Cat # BIO200
Fluorescent FITC conjugated peptides	This manuscript	Table S2
SARS-CoV-2 S HLAII epitopes	This manuscript	Tables S3 and S5
NEO-PV-01 HLA II epitopes	This manuscript	Table S7
Viral peptide	This manuscript	Table S7
Critical commercial assays		
Expi293™ Expression System Kit	ThermoFisher	Cat # A14635
ExpiCHO™ Expression System Kit	ThermoFisher	Cat # A29133
Pan T cell Isolation Kit, human	Miltenyi Biotec	Cat # 130-096-535
Chromium Next GEM Single Cell 5' Kit v2, 4 rxns	10X Genomics	Cat # 1000265
Chromium Next GEM Chip K Single Cell Kit, 16 rxns	10X Genomics	Cat # 1000287
Library Construction Kit, 16 rxns	10X Genomics	Cat # 1000190
5' Feature Barcode Kit, 16 rxns	10X Genomics	Cat # 1000256
Chromium Single Cell Human TCR Amplification Kit, 16 rxns	10X Genomics	Cat # 1000252

(Continued on next page)

Continued		
REAGENT or RESOURCE	SOURCE	IDENTIFIER
MiSeq Reagent Kit v2 (500-cycles)	Illumina	Cat # MS-102-2003
MiSeq Reagent Kit v2 (300-cycles)	Illumina	Cat # MS-102-2002
Experimental models: Cell lines		
Expi293F™ Cells	ThermoFisher	Cat # A14528
ExpiCHO-S™ Cells	ThermoFisher	Cat # A29127
Recombinant DNA		
pcDNA™3.4 TOPO™ TA	ThermoFisher	Cat # A14697
Software and algorithms		
Unicorn software v7.1	Cytiva	N/A
Liberty Blue operating Application Software v1.50.5913.17379	CEM	N/A
Liberty Prime operating Application Software v3.16.7711.19275	CEM	N/A
Waters MassLynx software v4.1	Waters	N/A
Waters Empower software v3 (feature release 4)	Waters	N/A
EnVision Manager v1.13	PerkinElmer	N/A
FACSDiva software v9.0	BD Biosciences	N/A
BD FACSAria software v8.0.1	BD Biosciences	N/A
MiSeq Control Software v2.6.2.1	Illumina	N/A
FloJo software v10.8	FlowJo Software (for Windows) Becton, Dickinson and Company; 2019.	https://www.flowjo.com/
GraphPad Prism v9	GraphPad Software, La Jolla California, USA	https://www.graphpad.com/
Cell Ranger software v6.0.1	10X Genomics	N/A
R package Seurat software v4.0.4	Main Reference #64	N/A
ComplexHeatmap R package	Main Reference #65	N/A
DescTools R package	Main Reference #66 Httpscrannr-Proj	https://cran.r-project.org/package=DescTools

RESOURCE AVAILABILITY

Lead contact

Further information and requests for resources and reagents should be directed to and will be fulfilled by the lead contact, John Srouji (john.srouji@biontech.us).

Materials availability

All unique/stable reagents generated in this study are available from the [lead contact](#) upon reasonable request with a completed Materials Transfer Agreement.

Data and code availability

- The datasets generated and analyzed in this study will be shared by the [lead contact](#) upon reasonable request.
- This paper did not report original code.
- Any additional information required to reanalyze the data reported in this paper is available from the [lead contact](#) upon reasonable request.

EXPERIMENTAL MODEL AND SUBJECT DETAILS

Healthy donor and patient samples

PBMCs from one melanoma, one NSCLC, and two bladder cancer patients (see [Table S6](#)) were collected and processed as part of a clinical trial evaluating a personalized neoantigen vaccine (NEO-PV-01) in combination with anti-PD-1 clinical trial (NCT02897765).⁴²

The study was conducted in accordance with the Declaration of Helsinki and with approval by the Institutional Review Board at each participating site and written informed consent was obtained for all patients. Information related to demographics (age, gender, disease status) can be found in [Table S6](#) and additional information related to patient samples and the clinical study has been previously published.⁴²

We selected convalescent COVID-19 PBMCs (from Precision for Medicine) from donors with >30 days between SARS-CoV-2 testing and blood draw (see [Table S4](#)). Donors were additionally pre-selected based on the presence of common HLA class II alleles. Purified PBMCs were frozen down at a concentration of $\sim 5.0 \times 10^6$ cells/mL. Peptides used in multimer analysis were selected using the following strategy: (a) prediction using an in-house algorithm²⁹ and/or previously reported^{35,36} SARS-CoV-2 epitopes. (b) Identification of allele restriction and binding affinities via the FP assay. For additional demographic information, please refer to [Table S4](#). These donors were not affiliated with a clinical study and, aside from COVID-19 infection, were otherwise disease-free.

Healthy donor leukopaks were sourced from the StemExpress Stem Cell Collection Center and PBMCs were isolated in-house (see [Table S6](#) for healthy donor information, including demographics). PBMCs were isolated using density gradient centrifugation in SepMate –50 (IVD) tubes (StemCell Technologies) containing Ficoll-Paque PLUS (GE). Blood collected from the leukopaks was diluted 1:1 with 1X PBS (Thermo Fisher). Twenty-five milliliters (25 mL) of blood was then carefully layered on top of 20 mL of Ficoll-Paque PLUS in each tube. Tubes were centrifuged at 1000xg for 20 min with the centrifuge deceleration brake off to prevent disruption of the Ficoll layer. Plasma and PBMCs were then collected in new 50 mL conical tubes and diluted 1:1 with 1X PBS. The tubes were centrifuged at 450xg for 5 min. The plasma supernatant was discarded and red blood cells in the PBMC pellet were removed by resuspending the cell pellet in 20 mL of ACK lysis buffer (Thermo Fisher) and incubating on ice for 5 min. Isolated PBMCs were then centrifuged at 450xg for 5 min, the supernatant was discarded, and cells were resuspended in RPMI GlutaMAX media (Thermo Fisher) supplemented with 10% (v/v) FBS. Cells were counted and resuspended in the appropriate amount of freeze media (FBS supplemented with 10% (v/v) DMSO) for vials at a 40×10^6 cell/vial concentration. CoolCell freezing containers (Corning) were used for controlled rate freezing at -80°C for 24 h and cells were then moved to the liquid nitrogen tank for long-term storage.

METHOD DETAILS

Soluble MHCII protein construct design, expression, and purification

Soluble MHC class II DNA construct design is based on Day et al.¹⁷ Each heterodimeric class II MHC allele is encoded with beta and alpha ectodomains separated by a P2A ribosomal skipping sequence and under the control of a constitutive CMV promoter (pcDNA3.4 – Thermo Fisher Scientific). Preceding each allele is its natural signal sequence for secretion into mammalian culture supernatant. At the N-terminus of the beta allele is a placeholder peptide (see [Table S1](#) for each allele-specific placeholder sequences) separated by a thrombin-cleavable linker peptide. Following each allele is a heterodimeric coiled coil motif (Jun following beta, Fos following alpha) and tag (biotin acceptor peptide (BAP) following beta, 10X-histidine tag following alpha).

Expi293F cells (Thermo Fisher Scientific) were cultured, maintained, and transiently transfected according to the manufacturer's recommendations in Optimum Growth Flasks (Thompson Instrument Company), shaking at 125 rpm with 8% CO₂. Briefly, healthy cells (grown at 37°C, $\geq 95\%$ viable, and at $\sim 3.0 \times 10^6$ cells/mL) were transfected with ExpiFectamine293 and the appropriate soluble MHCII construct DNA at a final concentration of 0.5 μg DNA per mL of culture and maintained at 32°C. Transfection kit enhancers 1 and 2 were added 18 h post-transfection at the recommended volumes. Cultures were harvested after 6 days of transient transfection via centrifugation at 16,000xg for 45 min at 4°C, after which the supernatant was filtered through a 0.22 μm regenerated cellulose membrane. Filtered supernatant was supplemented with 40 mM Tris-HCl pH 8.0, 300 mM NaCl, 23% (v/v) glycerol, and 1 mM PMSF prior to protein purification.

Soluble MHCII protein was purified from the media using HisTrap Excel media on an AKTA Pure running Unicorn software v7.1 (Cytiva). After sample application, IMAC media was washed with 20 column volumes (CV) of wash buffer (25 mM Tris-HCl pH 8.0, 300 mM NaCl, 10% (v/v) glycerol, 15 mM imidazole, pH 8.0) and protein eluted with 5 CV of elution buffer (25 mM Tris-HCl pH 8.0, 300 mM NaCl, 10% (v/v) glycerol, 250 mM imidazole, pH 8.0). Protein-containing fractions were subsequently pooled, concentrated, and desalted into 1X PBS using a HiPrep 26/10 Desalting column (Cytiva). Desalted protein was pooled and simultaneously digested with bovine thrombin (Sigma-Aldrich; 0.3 U thrombin per 10 μg of MHCII protein) and biotinylated with in-house produced *E. coli* BirA (5.5 μg BirA per 10 nmol of MHCII protein; final MHCII protein concentration in reaction $\leq 15 \mu\text{M}$) overnight at room temperature. Digested and biotinylated MHCII protein was finally purified via size exclusion chromatography using a Superdex 200 10/300 GL increase column (Cytiva) equilibrated with 1X PBS +16% (v/v) glycerol. Fractions corresponding to the low post-translationally modified population (typically centered at ~ 13 mL retention volume) were identified via SDS-PAGE, pooled, and concentrated using Amicon Ultracel 30K MWCO regenerated cellulose devices to ~ 2 mg/mL. Aliquots of 50 μL were snap frozen in liquid nitrogen and stored at -80°C until peptide exchange and multimer staining.

Soluble HLA-DM construct design, expression, and purification

The HLA-sDM DNA construct is designed similarly to the soluble MHCII construct (also inserted into pcDNA3.4). HLA-DMB and HLA-DMA ectodomains were fused to C-terminal biotin acceptor peptide (BAP) or 10X-histidine tags, respectively, and separated by an F2A ribosomal skipping sequence. Both ectodomains were linked to N-terminal secretion signal sequences^{62,63} to promote secretion

into the culture media. ExpiCHO-S cells (Thermo Fisher Scientific) were cultured, maintained, and transfected according to manufacturer's recommendations for Maximum Titer in Optimum Growth Flasks (Thompson Instrument Company) at 125 rpm shaking with 8% CO₂. Briefly, healthy cells (grown at 37°C, ≥95% viable, and ~6.0 × 10⁶ cells/mL) were transfected with ExpiFectamine CHO reagent and HLA-sDM construct DNA at a final concentration of 1.0 μg DNA per mL culture and maintained at 37°C for 18 h. Per the manufacturer's recommendations, ExpiFectamine CHO kit enhancers 1 and 2 were subsequently added and the culture transferred to 32°C. On day 5 post-transfection, ExpiCHO Feed was added to the culture and maintained at 32°C for another 9 days (14 days total). The culture was harvested via centrifugation at 16,000xg for 45 min at 4°C, after which the supernatant was filtered through a 0.22 μm regenerated cellulose membrane. Filtered supernatant was supplemented with 40 mM Tris-HCl pH 8.0, 300 mM NaCl, 23% (v/v) glycerol, and 1 mM PMSF prior to IMAC protein purification using HisTrap Excel media (Cytiva), as described above for soluble MHCII proteins. Protein-containing IMAC elution fractions (as determined by SDS-PAGE) were pooled and concentrated using Amicon Ultracel 30K MWCO regenerated cellulose devices to ~8 mg/mL. Final purification yield is typically ~20 mg/L transfected culture. Aliquots of 50 μL were snap frozen in liquid nitrogen and stored at –80°C until peptide exchange.

MHCII FITC-peptide probe synthesis and purification

To reduce FITC degradation, exposure to light was minimized during all steps of synthesis and purification. FITC-labeled peptide probes were synthesized using Fmoc-protected amino acids and a solid-phase peptide synthesis (SPPS) strategy on a CEM Liberty Blue HT24 microwave synthesizer operating Application Software v1.50.5913.17379 and CEM Liberty Prime instrument operating Application Software v3.16.7711.19275. Fmoc-Lys(IvDde)-OH was incorporated at the desired FITC-label position during synthesis for each specific sequence (see Table S2). After sequential amino acid addition was complete, all peptides were acetylated at the N-terminus by using acetic anhydride and diisopropylethylamine (DIEA) in N-methylpyrrolidone (NMP) and dimethylformamide (DMF), followed by Lys(IvDde) side chain deprotection with hydrazine in DMF. An equimolar quantity of fluorescein-5-isothiocyanate in DMF was added to the deprotected peptide resin along with DIEA to label the free lysine side chain at room temperature for 1–2 h. Afterward, peptide was cleaved from the solid support (using 95% trifluoroacetic acid (TFA), 2.5% water, 2.5% triisopropylsilane (TIS)) at room temperature, washed and precipitated in cold diethyl ether, reconstituted in 1:1 acetonitrile:water, and lyophilized.

FITC-labeled peptides were purified via reverse phase HPLC on a Waters Autopurification System with Waters 2767 Sample Manager and Waters SQD2 Mass Spectrometer operating Waters MassLynx software v4.1 and a Phenomenex Luna C₁₈ purification column (100Å, 10μm, 30 mm × 250 mm). For each peptide, a specific elution gradient of 0.05% TFA in water (mobile phase A) and 0.05% TFA in acetonitrile (mobile phase B) was used. After elution, fractions were immediately pooled, frozen, and lyophilized for at least 48 h. Peptide purity and molecular weight were determined by UPLC/MS on a Waters H-Class UPLC with PDA UV detector (at the wavelength of 214 nm) and QDa mass detector operating Waters Empower software v3 (feature release 4) and Waters Acquity UPLC Peptide BEH C₁₈ analytical column (130Å, 1.7μm, 2.1 mm × 100 mm). The UPLC mobile phases A and B were 0.100% TFA in water and 0.085% TFA in acetonitrile, respectively, with a flow rate of 0.50 mL/min. All peptides were purified to ≥88% purity. FITC-peptides were stored as lyophilized powder at –80°C until reconstitution in 100% DMSO at 10 mM immediately before use.

Fluorescence polarization (FP) assay

Fluorescence polarization (FP) based assays were developed to either assess the effect of catalysts on peptide exchange (direct loading of FITC-probes) or the IC₅₀ of putative epitope peptides (competition assay). For assessing the loading kinetics of FITC-peptide probes, soluble MHCII protein (125 nM) was incubated with 20 nM of the corresponding allele-specific FITC-peptide FP probe (see Table S2) in either assay buffer alone (100 mM sodium acetate pH 5.2, 50 mM NaCl, 0.01% (v/v) Tween 20), or in combination with either 0.2% (w/v) octyl glucoside or 187.5 nM HLA-sDM in a final reaction volume of 45 μL in a 384-well Optiplate (Perkin Elmer). The plate was incubated at 37°C and fluorescence polarization measured after 5 min, 1, 4, and 24 h, as described below for the competition assay.

For measuring the IC₅₀ of putative epitope peptides, MHCII protein (at an allele-specific concentration; Table S2), its corresponding FITC-peptide FP probe (at an allele-specific concentration; Table S2), HLA-sDM protein (at 1.5x [MHCII protein]), and an epitope peptide were incubated in assay buffer in a 384-well Optiplate at 37°C for 18 h. Fluorescence polarization was measured using an EnVision 2104 Multilabel Plate Reader (operating EnVision Manager v1.13) and “Optimized FITC FP Dual Emission Label” optics (Perkin Elmer) at 480 nm excitation and 535 nm emission wavelengths.

Percent bound peptide was calculated using the following formula:

$$\left\{ \left[1 - \frac{\text{sample}_{FP} - \text{free}_{FP}}{\text{no peptide}_{FP} - \text{free}_{FP}} \right] \right\} \times 100\%$$

where “*sample_{FP}*” is the fluorescence polarization value for the MHCII + FITC-probe + epitope condition, “*free_{FP}*” is the fluorescence polarization value of the FITC-probe alone, and “*no peptide_{FP}*” is the fluorescence polarization value for the MHCII + FITC-probe condition (note that HLA-sDM is present across all conditions). Graphpad Prism v9 was used for data analysis. Percent bound peptide versus log₁₀ peptide concentration were fit using the equation:

$$Y = \text{Bottom} + \frac{(\text{Top} - \text{Bottom})}{(1 + 10^{((\text{LogIC}_{50} - X) \cdot \text{HillSlope}))}}$$

where “Bottom” and “Top” are lowest and highest percent bound, X is \log_{10} peptide concentration and IC_{50} is 50% inhibition concentration.

Immunoprecipitation for epitope loading efficiency

MHCII protein alleles were loaded with FITC labeled peptides in presence of HLA-sDM as described in the previous section. Briefly, 10 μ M of MHCII protein was incubated with 100 μ M of FITC-labelled peptide in exchange buffer (100 mM sodium acetate pH 5.2, 50 mM NaCl, and 5 μ M HLA-sDM) for 18 h at 37°C. As a negative control for no epitope loading, MHC II protein was incubated in exchange buffer without any FITC-probe. Post-reaction samples were purified via size exclusion chromatography using a Superdex 200 10/300 GL increase column (Cytiva) in 1X PBS as described for MHCII protein purification. The SEC fractions containing MHCII protein were pooled as described for MHCII protein purification above and concentrated prior to immunoprecipitation (IP). In preparation for IP, 30 μ g of FITC monoclonal antibody (clone #1F8-1E4, ThermoFisher) was captured on 50 μ L of Gammabind Plus Sepharose (Cytiva) slurry in PBST buffer (1X PBS +0.01% (v/v) Tween 20) for 1 h at room temperature. Following incubation, the beads were washed and incubated with 10 μ g of SEC-purified post-exchange MHCII protein samples in PBST for 1 h at room temperature. The beads were centrifuged at 300xg for 1 min and flow through were collected. Both immunoprecipitation (IP) load and flow through were reduced, denatured, and analyzed on 10% Criterion XT Bis-Tris Protein Gel (BIO-RAD) to determine how much MHCII protein remained unloaded with FITC-probe post-exchange with HLA-sDM.

Analytical SEC of MHCII protein stability

To assess the appearance of MHCII protein aggregates over time due to storage, samples were subjected to a defined number of freeze/thaws and analyzed for the presence of a void fraction peak via analytical SEC on an HPLC instrument. A Phenomenex BioSep 5 μ m SEC-s4000 500 Å LC column was used on an Agilent HPLC with 1260 Infinity II Bio-inert Pump and 1260 Infinity II MW Detector operated by OpenLab CDS workstation v2.7. MHCII protein samples were diluted to 1 μ M, loaded onto the column equilibrated with PBS and monitored via OD_{230} at 1 mL/min. High molecular weight aggregates were monitored at a retention time of 5.5 min.

Epitope loading for multimer analysis

Epitopes for convalescent COVID-19 donor analysis were initially selected based on a combination of neon-mhc2 predictions²⁹ and previously reported reactivities,^{35,36} allele restrictions were subsequently determined using the FP assay. MHCII alleles were loaded with epitopes via HLA-sDM catalysis as described above (epitope lengths ranged from 15–17 amino acids long; stocks were stored in 100% DMSO at 10 mM). In a 96-well polypropylene microtiter plate, 5 μ M soluble MHCII protein (henceforth referred to as “monomer”) was incubated in exchange buffer (100 mM sodium acetate pH 5.2, 50 mM NaCl, and 5 μ M HLA-sDM) with 100 μ M epitope peptide (dissolved in 100% DMSO) in a final volume of 100 μ L. Epitope-loading reactions proceeded overnight at 37°C in a 96-well plate to ensure complete peptide exchange across all alleles considered. After incubation, the plate was centrifuged at 3300xg for 10 min to remove aggregates, and the supernatant transferred and neutralized with 2X PBS final concentration. Exchanged pMHCII monomers were either freshly conjugated with fluorochrome-labeled streptavidin (see below) or stored unconjugated at –80°C until future use.

MHCII multimerization, staining, and activation panel

During all steps of multimerization and staining, care was taken to shield the samples from light. Combinatorial coding^{33,34} was applied for simultaneous *ex vivo* detection of multiple pMHCII reactivities in PBMC samples via flow cytometry. Exchanged pMHCII monomers (at 0.1 mg/mL or 1.6 μ M) were incubated with fluorochrome-conjugated streptavidin (SA) at a 4:1 pMHCII:SA molar ratio on ice for 30 min. Afterward, 25 μ M free biotin was added to block any unoccupied SA binding sites and incubated on ice for 10 min. Multimers were subsequently centrifuged at 3300xg for 10 min to remove aggregates and the resulting supernatants were subsequently pooled appropriately.

PBMCs were thawed and treated with 0.025 U/ μ L benzonase and 50 nM dasatinib (Sigma-Aldrich) at 37°C for 20 min in RPMI media supplemented with 10% (v/v) FBS. Afterward, PBMCs were centrifuged at 450xg for 5 min and washed once in FACS buffer (1X PBS, 0.5% (w/v) BSA, 50 nM dasatinib). PBMCs were then resuspended with the pooled multimer mixture in a final staining volume of 50 μ L for up to 3 million cells per sample with FACS buffer. Samples were incubated with multimers at 37°C for 1 h, and subsequently stained with the appropriate surface antibodies for 30 min on ice (see [key resources table](#)). After incubation, samples were washed twice with FACS buffer and resuspended in 200 μ L FACS buffer. Samples were acquired on a BD LSR Fortessa X-20 instrument equipped with 355, 405, 488, 561, and 640 nm lasers and FACSDiva software version 9.0.

Flow cytometry analysis

Combinatorial coding³³ was applied whenever possible, in which each pMHCII antigen is conjugated to two distinct streptavidin fluorophores. Up to four different streptavidin fluorophores were used to analyze up to six different pMHCII color combinations in a single pool. Streptavidin based PE, APC multimers were used at 0.5 μ g/mL while PE-CF594 and BV711 multimers were used at 0.4 and 2 μ g/mL respectively. To identify a positive multimer response, the following strategy was applied: (a) Selection of CD4⁺ cells (see [Figures S5A and S6A](#) for full gating strategies). (b) Selection of CD4⁺ T cells that were specifically double-positive for the two different streptavidin fluorophores assigned to the relevant epitope and negative for the other two colors via Boolean gating. This selected

population was overlaid on the total CD4⁺ population. (c) A multimer frequency of $\geq 0.001\%$ (of CD4⁺) with at least ten events. Positive multimer responses were confirmed with a second and separate multimer staining where at least one of the streptavidin fluorophores from the initial staining was changed to a different fluorophore. For low-frequency antigen-specific CD4⁺ T cell populations, some variation in measured multimer positive frequencies may be observed within the same patient/donor due to PBMC vial-to-vial variation. The irrelevant peptide control for every MHCII allele was included in the confirmation staining to assess background staining. FlowJo software (FlowJo v10.8) was used for data analysis.

T cell induction in healthy donor samples

For T cell inductions, healthy donor human PBMCs were stimulated with peptide as described previously.³⁰ Briefly, PBMC were incubated with viral peptides (influenza (HA₁₃₀₆₋₃₁₈), CMV (pp65₁₁₆₋₁₂₉), and HIV (Gag₂₆₂₋₂₇₆)), cultured in presence of IL-7 and IL-15 (CellGenix GmbH, Germany), matured, and harvested.

Cell sorting and CITEseq antibody labeling

PBMCs from patient NSCLC-L7 were thawed and T-cells were isolated using the human Pan T cell Isolation Kit (Miltenyi Biotec) according to manufacturer's recommendations. Isolated T cells were treated with 0.025 U/ μ L benzonase and 50 nM dasatinib (Sigma-Aldrich) in RPMI media supplemented with 10% (v/v) FBS. Cells were centrifuged at 450xg for 5 min and washed once with FACS buffer. Cells were resuspended in a pooled multimer mix made in FACS buffer at a final volume of 50 μ L for up to 3 million cells before incubating with multimers for 45 min at 37°C. CCR7 and CXCR5 TotalSeq-C antibodies (Biolegend) were added to the cells and incubated at 37°C for 15 min. Cells were then stained with Live/Dead dye (Near IR) and a panel of 17 TotalSeq-C surface antibodies (Biolegend, [key resources table](#)) and incubated for 30 min on ice. After incubation, cells were washed twice with FACS buffer and resuspended in 200 μ L of FACS buffer. Cells were analyzed on a BD FACS Aria Fusion cell sorter equipped with 405, 488, 561, and 640 nm lasers and FACSDiva software version 8.0.1. For patient NSCLC-L7, four different CD4⁺ (Live CD3⁺ CD4⁺ CD8⁻) T cell populations were sorted: bulk, ASP0064 + DRB1*07:01, ASP0034 + DRB1*07:01, and ASP0043 + DRB1*12:01 (see [Figure S6A](#) for full gating strategy).

Single-cell TCR and surface epitope sequencing

Aria cell counts were used to determine the total number of cells sorted for each population. Sorted cells were processed for TCR V(D)J sequencing (Chromium Next GEM Single Cell 5' Reagent Kits v2 (Dual Index), 10X Genomics), according to manufacturer's recommendations. After Gel beads-in-EMulsion Reverse Transcription (GEM-RT) reaction and clean-up, PCR amplification was performed to generate subsequent libraries for sequencing. V(D)J library (Chromium Single Cell Human TCR Amplification Kit) and cell surface protein library (5' Feature Barcode Kit) were prepared according to manufacturer's recommendations. cDNA libraries were QC-ed using the Bioanalyzer and Agilent High Sensitivity DNA Kit. Sequencing libraries were quantified using KAPA Library Quantification Kits - Complete kit and the LightCycler 480 (Roche). The libraries for all the four sorted populations were pooled and sequenced on the Illumina MiSeq platform operating MiSeq Control Software v2.6.2.1.

QUANTIFICATION AND STATISTICAL ANALYSIS

Single cell CITE/TCR analysis

Cell Ranger version 6.0.1 (10X Genomics) was used to align raw sequencing data from the CITE library with the 'count' option selected, using a custom panel of antibodies. R package Seurat 4.0.4⁶⁴ was used for downstream analysis of data acquired from the Cell Ranger count. We filtered cells that had more than 3000 unique molecular identifiers (UMI). Data was normalized using the CLR method⁶⁴ scaled by the ScaleData function using all available antibodies (except for CTLA4, KLRG1, 41BB, LAMP1, TIM3, CX3CR1, HLA Class II and CD57, which had low expression and off-target binding) and analyzed using principal component analysis (PCA). A UMAP dimensionality reduction was performed using the first 15 PCA to obtain a two-dimensional representation of the cell states. For clustering, we applied the FindClusters function with resolution of 0.6. For heatmap representation we used mean expression of protein markers inside each cluster. Heatmaps were built with ComplexHeatmap R package.⁶⁵ To analyze TCR clonality, we excluded all TCR sequences that did not correspond to a cell barcode in the CITE library (post quality control). Gini coefficients were computed using the DescTools R package.⁶⁶

Statistical analysis

All analyses were performed in either the R language and environment for statistical computing (version 4.0.4) or GraphPad Prism (version 9). Likewise, all figures were created using an R script on the "ggplot2" package⁶⁷ or GraphPad Prism. All the statistical details of experiments can be found in the figure legends and results, including the statistical test used and sample size for each experiment.